Mon. Not. R. Astron. Soc. **387,** 1345–1360 (2008) doi:10.1111/j.1365-2966.2008.13003.x

Constraining dark matter properties with SPI

Alexey Boyarsky,[1⋆] Denys Malyshev,[2,3]† Andrey Neronov[4,5⋆] and Oleg Ruchayskiy[6]

[1]*CERN, PH/TH, CH-1211 Geneve 23, Switzerland*
[2]*Bogolyubov Institute for Theoretical Physics, Kiev, 03780, Ukraine*
[3]*Dublin Institute for Advanced Studies, 31 Fitzwilliam Place, Dublin 2, Ireland*
[4]*INTEGRAL Science Data Centre, Chemin d'Écogia 16, 1290 Versoix, Switzerland*
[5]*Geneva Observatory, 51 ch. des Maillettes, CH-1290 Sauverny, Switzerland*
[6]*École Polytechnique Fédérale de Lausanne, Institute of Theoretical Physics, FSB/ITP/LPPC, BSP 720, CH-1015, Lausanne, Switzerland*

Accepted 2008 January 22. Received 2008 January 14; in original form 2007 November 14

ABSTRACT

Using the high-resolution spectrometer SPI on board the *International Gamma-Ray Astrophysics Laboratory* (*INTEGRAL*), we search for a spectral line produced by a dark matter (DM) particle with a mass in the range 40 keV $< M_{\rm DM} <$ 14 MeV, decaying in the DM halo of the Milky Way. To distinguish the DM decay line from numerous instrumental lines found in the SPI background spectrum, we study the dependence of the intensity of the line signal on the offset of the SPI pointing from the direction toward the Galactic Centre. After a critical analysis of the uncertainties of the DM density profile in the inner Galaxy, we find that the intensity of the DM decay line should decrease by at least a factor of 3 when the offset from the Galactic Centre increases from 0° to 180°. We find that such a pronounced variation of the line flux across the sky is not observed for any line, detected with a significance higher than 3σ in the SPI background spectrum. Possible DM decay origin is not ruled out only for the unidentified spectral lines, having low ($\sim 3\sigma$) significance or coinciding in position with the instrumental ones. In the energy interval from 20 keV to 7 MeV, we derive restrictions on the DM decay line flux, implied by the (non-)detection of the DM decay line. For a particular DM candidate, the sterile neutrino of mass $M_{\rm DM}$, we derive a bound on the mixing angle.

Key words: methods: data analysis – techniques: spectroscopic – Galaxy: halo – dark matter.

1 INTRODUCTION

1.1 Dark matter in the Universe

There is a vast body of evidence suggesting that a large fraction of matter in the Universe exists in the form of dark matter (DM). However, while the total density of DM is measured with very high precision ($\Omega_{\rm DM}h^2 = 0.105^{+0.007}_{-0.009}$; Spergel et al. 2007), little is known about its properties apart from this. The possibility that DM is composed of standard model (SM) particles has been ruled out for a long time already. Indeed, DM cannot be made out of baryons, as producing such an amount of baryonic matter would require drastic modifications to the scenario of the big bang nucleosynthesis (BBN), which otherwise successfully describes the abundance of light elements (see, for example, Dar 1995). Recent microlensing experiments rule out the possibility that another type of baryonic DM – massive compact halo objects (MACHOs) – constitutes a dominant fraction of mass in the halo (Alcock et al. 2000; Lasserre et al. 2000; Alard 1999). The only non-baryonic DM candidate in the SM candidates – the (left-handed) neutrino – is ruled out by large-scale structure (LSS) considerations (see, for example, Bond, Efstathiou & Silk 1980; Hannestad & Raffelt 2004; Crotty, Lesgourgues & Pastor 2004).

What are the properties of a successful DM candidate? First of all, this particle should be massive. Many extensions of the SM present DM candidates with masses ranging from $\sim 10^{-10}$ eV (massive gravitons; Dubovsky, Tinyakov & Tkachev 2005) and $\sim 10^{-6}$ eV (axions) to hundreds of GeV (weakly interacting massive particles, WIMPs) and even to 10^{13} GeV (WIMPZILLA; Kuzmin & Tkachev 1998, 1999; Chung, Kolb & Riotto 1999). For a review of particle physics DM candidates, see, for example, Bergstrom (2000), Bertone, Hooper & Silk (2005) and Carr, Lamanna & Lavalle (2006).

Secondly, there should exist mechanisms of DM production with the correct abundances. The production mechanism, in particular, determines the velocity distribution of particles in the early Universe. This velocity distribution can, in principle, be probed experimentally. Namely, if during the structure formation epoch

⋆On leave of absence from Bogolyubov Institute for Theoretical Physics, Kiev, Ukraine.
†E-mail: dmalishev@gmail.com

the DM particles have velocities comparable to the speed of sound in the baryon–photon plasma, they 'erase' density fluctuations at scales smaller than the distance they have travelled (called the free-streaming length). To differentiate various models in accordance with this property, DM candidates with negligible velocity dispersion (and, correspondingly, free-streaming) are called cold dark matter (CDM), while those with free-streaming of the order of $\sim$1 Mpc are considered to be warm dark matter (WDM).[1] It is possible to constrain the free-streaming length of a particular DM candidate by probing the structure of the Universe at galaxy-size scales. This can be done through the analysis of the Lymanα (Lyα) forest data (Hui, Gnedin & Zhang 1997). Lyα analysis puts an upper bound on the free-streaming of DM particles (Hansen et al. 2002; Viel et al. 2005; Seljak et al. 2006; Viel et al. 2006, 2008). It should be noted, however, that the currently existing interpretation of the Lyα data is model-dependent. Apart from a number of astrophysical assumptions (see Hui et al. 1997) and complicated hydrodynamic simulations, it relies on a priori assumptions about the velocity distribution of DM particles.

A way to differentiate between CDM and WDM models would be to compare the numerical simulations of the DM distribution in Milky-Way-type galaxies with the actual observations. However, the resolution of N-body simulations is not yet sufficient to answer questions about, for example, the DM density profiles in dwarf satellite galaxies. Moreover, most of the simulations include only collisionless DM particles, and do not model the baryons and their feedback on the galaxy structure formation. These problems are not solved even for CDM simulations, and WDM simulations have additional serious difficulties. From an observational point of view, it has been argued for some time already that there is a discrepancy between CDM simulations and observations (see, for example, Moore 1994; Klypin et al. 1999; Moore et al. 1999; Bode, Ostriker & Turok 2001; Avila-Reese et al. 2001; Goerdt et al. 2006) It has been claimed recently that a number of recent observations of dwarf satellite galaxies of the Milky Way and Andromeda galaxy seem to indicate the existence of the smallest scale at which DM exists (Gilmore et al. 2007a,b; Gilmore 2007; Koposov et al. 2007). However, this statement and the interpretation of the observations are still subject to debate (Klimentowski et al. 2007; Penarrubia, McConnachie & Navarro 2007; Simon & Geha 2007; Strigari et al. 2007). Therefore, it is too early to say what type of DM model is favoured by comparing simulations and observations.

Usually, it is also necessary for the DM candidate to be stable. For the most popular DM candidate, WIMPs, this is related to the fact that particles of $\sim$ electroweak mass, which have a weak strength interaction with SM matter (required to produce the correct amount of DM), would decay too fast and would not be 'dark'. If, however, the DM particle interacts with the SM more weakly than WIMPs, it could well have a finite (although cosmologically long) lifetime.

There are several unstable (decaying) DM candidates, e.g. the gravitino (Borgani, Masiero & Yamaguchi 1996; Baltz & Murayama 2003; Roszkowski, Ruiz de Austri & Choi 2005; Cembranos et al. 2006; Cerdeno et al. 2006; Lola, Osland & Raklev 2007). In this paper, we concentrate mainly on one candidate, the sterile neutrino (although our results are applicable for any type of decaying DM). Constraints on the decaying DM have been analysed in de Rujula & Glashow (1980), Berezhiani, Vysotsky & Khlopov (1987), Doroshkevich, Khlopov & Klypin (1989), Berezhiani et al. (1990), Berezhiani & Khlopov (1990) and Bertone et al. (2007); Zhang et al. (2007); see also the book by Khlopov (1997).

1.2 Sterile neutrino dark matter

It was noticed long ago that the right-handed (or as it is often called 'sterile') neutrino with mass in the keV range could represent a viable DM candidate (Dodelson & Widrow 1994). Such a neutrino could interact with the rest of matter only via quadratic mixing with left-handed ('active') neutrinos, and therefore (although not stable) could have a cosmologically long lifetime. At the same time, it could have been produced in the early Universe with the correct abundances (Dodelson & Widrow 1994; Shi & Fuller 1999; Shaposhnikov & Tkachev 2006). One of the decay channels of unstable sterile neutrinos includes the emission of photons with energy equal to half of the sterile neutrino rest energy. Potentially, this makes it possible to observe the decays of DM sterile neutrinos using the detection of a characteristic spectral line in the spectra of astrophysical objects with a large DM concentration.

Recently, this DM candidate has attracted much attention (see, for example, Shaposhnikov 2007, and references therein). It was found that a very modest and natural extension of the SM by three right-handed neutrinos (making the SM more symmetric as all SM fermions, including the neutrino, would have now their left- and right-handed counterparts) provided a viable extension of the theory, capable of solving several 'beyond the SM' problems. First of all, such an extension makes neutrinos massive and thus perhaps provides the simplest and most natural explanation of the phenomenon of 'neutrino oscillations' (for reviews, see, for example, Fogli et al. 2006; Strumia & Vissani 2006; Giunti 2007). The smallness of neutrino masses in this model (called the νMSM in Asaka & Shaposhnikov 2005) is achieved by the usual seesaw mechanism with Majorana masses of right-handed neutrinos being below the electroweak scale.[2]

Secondly, if two heavier sterile neutrinos (N_2 and N_3) are almost degenerate in mass and have their masses between $\mathcal{O}(100)$ MeV and $\mathcal{O}(20)$ GeV, the νMSM provides the mechanism for generating the baryon asymmetry of the Universe. Thirdly, the lightest sterile neutrino, N_1, can have arbitrary mass and arbitrarily weak coupling with the (active) neutrino sector. At the same time, it can be produced in the early Universe in the correct amounts. Therefore, it represents the DM particle in the νMSM. Thus, altogether the νMSM represents (arguably) the simplest extension of the SM, capable of explaining three important questions: the origin and smallness of neutrino masses, the baryon asymmetry in the Universe and the existence of DM.

1.3 Existing restrictions on sterile neutrino dark matter parameters

What are the current restrictions on parameters (mass and mixing) of sterile neutrino DM? First of all, sterile neutrino mass

[1] The left-handed neutrino would represent hot DM in this terminology (i.e. DM with a free-streaming length $\gg$1 Mpc).

[2] The fact that the νMSM does not introduce any new scale above the electroweak scale makes this theory especially appealing from the point of view of its experimental verification/falsification.

should satisfy the universal Tremaine–Gunn lower bound:[3] $M_{\rm DM} \gtrsim$ 300–500 eV.[4]

Next, as the sterile neutrino possesses a (two-body) radiative decay channel, $N_1 \rightarrow \nu + \gamma$, the emitted photon would carry the energy $E_\gamma = M_{\rm DM}/2$. A large flux of such photons is expected from large concentrations of DM sterile neutrinos, such as galaxies or galaxy clusters.

Recently, an extensive search of the DM decay line in the region of masses $M_{\rm DM} \lesssim 20$ keV was conducted, using the data of *Chandra* (Riemer-Sørensen, Hansen & Pedersen 2006; Boyarsky, Ruchayskiy & Markevitch 2006d; Abazajian et al. 2007) and *XMM–Newton* (Boyarsky et al. 2006a,b,c; Watson et al. 2006; Boyarsky, Nevalainen & Ruchayskiy 2007a). The soft X-ray region (down to energies of 0.2 keV) was explored by Boyarsky et al. (2007b) with the use of the wide field of view (FOV) spectrometer (McCammon et al. 2002). The non-observation of the DM decay line in X-ray, combined with the first principles calculation of DM production in the early Universe (Asaka, Laine & Shaposhnikov 2007), implies that the Dodelson & Widrow (1994, DW) scenario can work only if the sterile neutrino mass is below 4 keV (Boyarsky et al. 2007c). If we take into account the recent lower bound on the mass of sterile neutrino DM in the DW scenario $M_{\rm DM} \geqslant 5.6$ keV (Viel et al. 2008), it seems that the possibility that all DM is produced via the DW scenario is ruled out (Boyarsky et al. 2007c). The possibility that only a fraction of the DM is produced via the DW mechanism remains open (Palazzo et al. 2007).

There are other viable mechanisms of DM production, including, for example, resonant oscillation production in the presence of lepton asymmetries (Shi & Fuller 1999). Sterile neutrino DM can be produced by the decay of the light inflaton (Shaposhnikov & Tkachev 2006) or in a similar model with a different choice of parameters (Kusenko 2006; Petraki & Kusenko 2008). These mechanisms are currently not constrained and remain valid for DM particles with masses in the keV range and above.

The search for the DM decay line signal produced by sterile neutrinos with masses above ∼20 keV is complicated by the absence of focusing optics telescopes (similar to *Chandra* or *XMM–Newton*) in the hard X-ray and γ-ray domain of the spectrum. For example, the existing restrictions in the 20–100 keV mass range (Boyarsky et al. 2006a,c) are derived from observations of the diffuse X-ray background, with the help of non-imaging instruments, such as the High Energy Astronomy Observatory I (HEAO-I; Gruber et al. 1999). The current status of astrophysical observations is summarized in Ruchayskiy (2007).

In this paper, we use the spectrometer SPI on board the *INTEGRAL* satellite to place restrictions on the parameters of decaying DM in the mass range from 40 keV to 14 MeV. This range of masses is interesting because of, for example, sterile neutrinos produced in the early Universe in the presence of large lepton asymmetries (Shi & Fuller 1999) or through the inflaton decay (Shaposhnikov & Tkachev 2006). It is also relevant for the case of gravitino DM (Pagels & Primack 1982; Bond, Szalay & Turner 1982).

When the preparation of this paper was at its final stage, Yuksel, Beacom & Watson (2007, hereafter Y07) published their work, which used the results of Teegarden & Watanabe (2006, hereafter TW06) to place restrictions on the parameters of sterile neutrino DM in the range 40–700 keV. We discuss this in more detail in Section 6.

1.4 SPI spectrometer

The absence of focusing optics significantly reduces the sensitivity of the telescopes operating in the hard X-ray/soft γ-ray energy band. Most of the instruments operating in this energy band use collimators and/or coded masks to distinguish signals from sources in the sky from the instrumental background. Contrary to focusing optics telescopes, both source and background signals are collected from the entire detector, which significantly increases the irreducible background.

The focusing optics enables us to significantly reduce the background only in the studies of point sources. If the source under investigation occupies a large fraction of the sky (e.g. the entire Milky Way galaxy), the performance of the focusing and non-focusing instruments with the same detector collection area are, in fact, comparable.

In the case of an extended source, emitting a narrow spectral line, an efficient way to reduce the instrumental background is by improving the spectral resolution of the instrument (in the case of a broad continuum background spectrum, the number of background counts at the energy of the line is proportional to the spectral resolution ΔE). The best possible sensitivity is achieved when the spectral resolution reaches the intrinsic width of the spectral line (see Fig. 1 for wide FOV instruments and Boyarsky et al. 2007b for narrow FOV instruments).

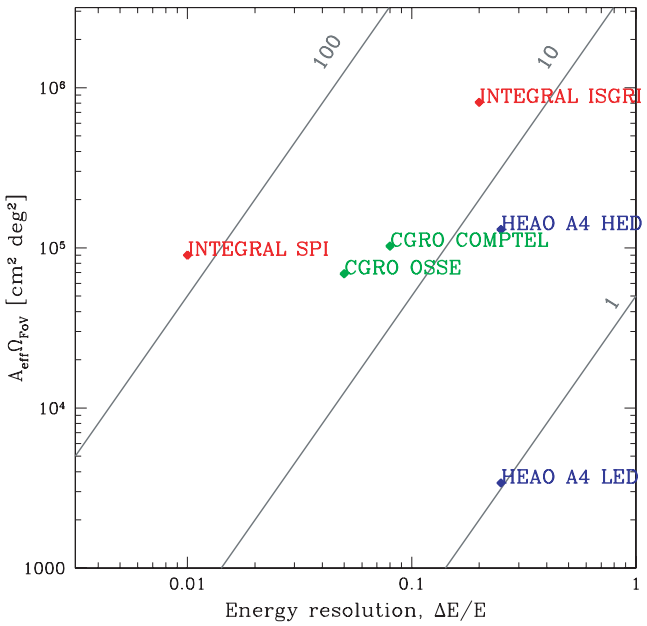

Figure 1. Comparison of sensitivity towards the search of the narrow DM decay line for different instruments with a wide FOV. Diagonal straight lines show the improvement of sensitivity (by a factor marked on the line) as compared with the HEAO-I A4 low-energy detector, taken as a reference.

[3] In its simplest form, the Tremaine–Gunn bound comes from the fact that for fermions there is a maximal density in the phase space (Tremaine & Gunn 1979; Dalcanton & Hogan 2001), and therefore the observed phase-space density in various DM-dominated systems should be less than this (mass-dependent) bound.

[4] A stronger lower bound from Lyα (Seljak et al. 2006; Viel et al. 2006, 2008) can be obtained for particular production mechanisms: the Dodelson–Widrow scenario (Dodelson & Widrow 1994). For other possible production mechanisms (e.g. Shi & Fuller 1999; Shaposhnikov & Tkachev 2006), the Lyα constraints should be re-analysed.

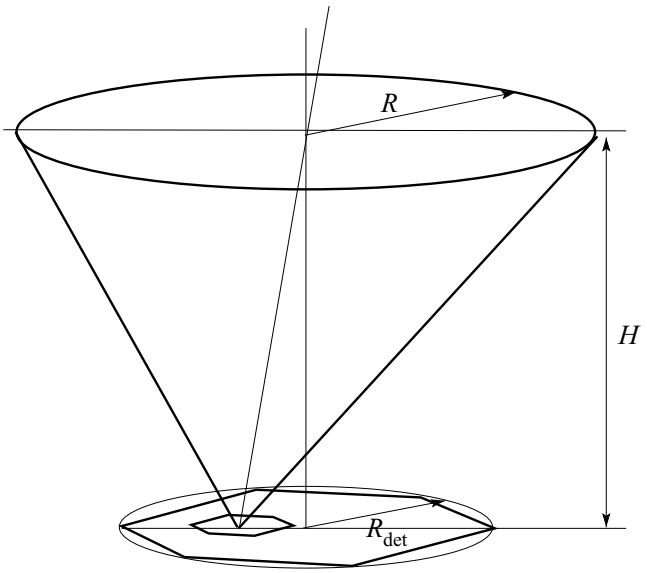

Figure 2. The geometry of the SPI FOV.

In the case of the line produced by the DM decaying in the Milky Way halo, the line width is determined by the Doppler broadening by the random motion of the DM particles. The velocity dispersion of the DM motion in the halo is about the rotation velocity of the Galactic disk, $v \sim 200$ km s^{-1}. This means that Doppler broadening of the DM decay line is about

$$\frac{\Delta E}{E} \sim \frac{v}{c} \simeq 10^{-3}. \tag{1}$$

Thus, the optimal spectral resolution of an instrument searching for the DM decay line produced by the Milky Way DM halo should be $\Delta E \simeq 10^{-3}\, E$.

Such optimal spectral resolution is almost achieved with the spectrometer SPI on board the *INTEGRAL* satellite, which has a maximal spectral resolving power of $E/\Delta E \simeq 500$ and works in the energy range from 20 keV to 8 MeV (Vedrenne et al. 2003). SPI is a 'coded mask' type instrument with an array of 19 hexagonal-shaped Ge detectors (of which only 17 are operating at the moment).

The SPI telescope consists of a coded mask inscribed into a circle of radius $R_{\rm mask} = 39$ cm, placed at a height of $H = 171$ cm above the detector plane, and of the detector, which has the shape of a hexagon inscribed into a circle of radius $R_{\rm det} \simeq 15.3$ cm (see Fig. 2). The portion of the sky visible from each point of the SPI detector (the so-called fully coded field of view, FCFOV) therefore has an angular diameter

$$\Theta_{\rm FCFOV} = 2 \arctan\left(\frac{R_{\rm mask} - R_{\rm det}}{H}\right) \approx 16^\circ. \tag{2}$$

The portion of the sky visible by at least some of the detectors (the PCFOV) is

$$\Theta_{\rm PCFOV} = 2 \arctan\left(\frac{R_{\rm mask} + R_{\rm det}}{H}\right) \approx 35^\circ. \tag{3}$$

The solid angle spanned by the cone with this opening angle is $\Omega_{\rm PCFOV} = 2\pi[1 - \cos(\Theta_{\rm PCFOV}/2)] \simeq 0.29$ (see Fig. 2). The wide FOV makes the SPI telescope suitable for studying very extended sources, such as the Milky Way DM halo.

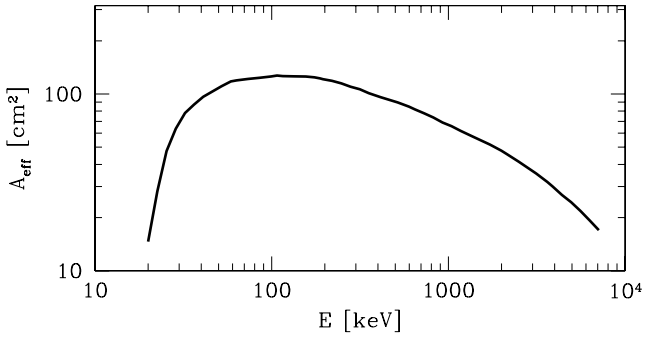

Figure 3. The effective area of the SPI detector for an on-axis source, as a function of the photon energy. The plot is produced by collecting the on-axis effective areas of the 17 SPI detectors from the instrumental characteristics files.

2 EXPECTED SIGNAL FROM DARK MATTER DECAY IN THE MILKY WAY HALO

The expected surface brightness of the DM decay line in a given direction on the sky is a function of the angular distance ϕ between the given direction on the sky and the direction towards the Galactic Centre (GC). This can be calculated by taking the integral of the DM density profile $\rho_{\rm DM}(r)$ along the line of sight ('column density')

$$\mathcal{S}_{\rm DM}(\phi) = \int_0^\infty {\rm d}z\, \rho_{\rm DM}\left(\sqrt{r_\odot^2 - 2 z r_\odot \cos\phi + z^2}\right), \tag{4}$$

where $r_\odot \simeq 8.5$ kpc is the distance from the Solar system to the GC. Angle ϕ is related to the galactic coordinates (b, l) via

$$\cos\phi = \cos b\, \cos l. \tag{5}$$

Thus, the galactic centre corresponds to $\phi = 0^\circ$, the anticentre $\phi = 180^\circ$ and the direction perpendicular to the galactic plane to $\phi = 90^\circ$. The expected DM flux is then given by

$$\frac{{\rm d}F_{\rm DM}(\phi)}{{\rm d}\Omega} = \frac{\Gamma_{\rm DM} E_\gamma}{4\pi M_{\rm DM}} \mathcal{S}_{\rm DM}(\phi), \tag{6}$$

where $\Gamma_{\rm DM}$ is the DM decay rate.

In general, the surface brightness $F_{\rm DM}(\phi)$ is variable across the telescope FOV. This is especially true for wide FOV instruments (such as SPI). In order to calculate the detector count rate, we must integrate flux (equation 6) over the FOV and over the (effective) detector area, and then divide by the energy of the photons, $E_\gamma = M_{\rm DM}/2$:

$$R = \iint_{\rm FOV} {\rm d}\alpha\, {\rm d}\beta \frac{A_{\rm eff}(E_\gamma\,|\,\alpha, \beta)}{E_\gamma} \frac{{\rm d}F_{\rm DM}}{{\rm d}\Omega}\left[\phi(\alpha, \beta)\right]. \tag{7}$$

Here, (α, β) are the angular coordinates in the FOV, and $A_{\rm eff}$ is the effective area at energy E_γ for photons coming from the direction (α, β).

The effective area of the SPI detector (which is determined by the transparency of the mask and the quantum efficiency of the detector) changes with the photon energy. For an on-axis point source,

$${\rm d}F/{\rm d}\Omega(\alpha, \beta) = f_0 \delta(\alpha)\delta(\beta),$$

the integral of equation (7) reduces to $f_0\, A_{\rm eff,on}$, where $A_{\rm eff,on}(E_\gamma)$ is the detector effective area for an on-axis source. Its dependence on energy E_γ is shown in Fig. 3.[5]

[5] The on-axis effective area is calculated by summing the energy-dependent on-axis effective areas of each of the 17 operating detectors of SPI, extracted from the instrument's characteristics files.

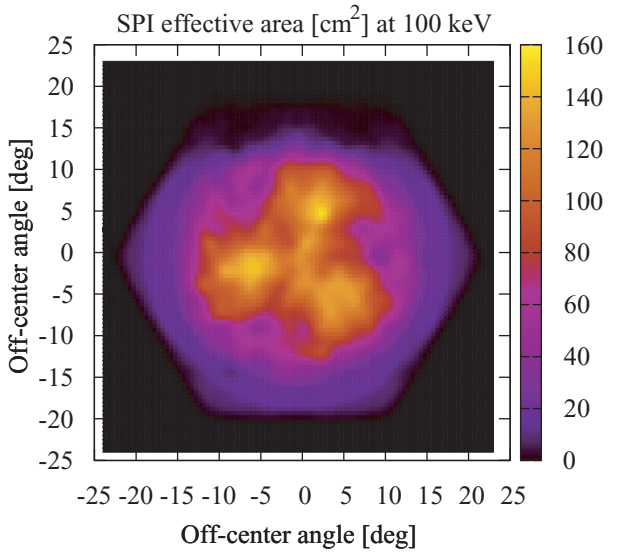

Figure 4. Dependence of the effective area on the off-axis position of a (point) source.

In the general case of extended sources, evaluation of the detector count rate (equation 7) analytically is not possible because of the complicated dependence of the effective area on the off-axis angle (shown in Fig. 4). In the simplest case of an extended source with a constant surface brightness $\mathrm{d}F_{\mathrm{DM}}(\phi)/\mathrm{d}\Omega = f_{\mathrm{ext}} = \mathrm{const}$, the integral of equation (7) reduces to the multiplication by the solid angle $\Omega_{\mathrm{PCFOV}} \simeq 0.29$ and the effective area, averaged over the FOV:

$$A_{\mathrm{eff,\,ext}}(E_\gamma) = \frac{1}{\Omega_{\mathrm{PCFOV}}} \iint_{\mathrm{FOV}} \mathrm{d}\alpha\, \mathrm{d}\beta\, A_{\mathrm{eff}}(E_\gamma\,|\,\alpha,\beta) \approx \kappa(E_\gamma) A_{\mathrm{eff,\,on}}(E_\gamma). \quad (8)$$

The numerical factor $\kappa(E_\gamma)$ depends on the energy and has to be calculated using numerical integration over the energy-dependent off-axis response map of the SPI detector. A reasonably accurate numerical approximation to $\kappa(E_\gamma)$ is given by

$$\kappa(E) \approx 0.165 (E\,\mathrm{keV}^{-1})^{0.11}. \quad (9)$$

We can see that $\kappa \ll 1$ in the whole energy interval. This is explained by the fact that the detector area visible from a given direction on the sky strongly decreases with the increase of the off-axis angle of this direction. Thus, the sky-averaged effective area is much smaller than the on-axis effective area of the detector. Substituting equations (8) and (9) into equation (7) we find that for an extended source of constant surface brightness the detector count rate is

$$R_{\mathrm{ext}} = 2.73 \times 10^{-5}\,\mathrm{cts\,s^{-1}} \left(\frac{1\,\mathrm{keV}}{E_\gamma}\right) \left[\frac{A_{\mathrm{eff,\,ext}}(E_\gamma)}{150\,\mathrm{cm}^2}\right] \times \left[\frac{(\mathrm{d}F_{\mathrm{DM}}/\mathrm{d}\Omega)_{\mathrm{ext}}}{10^{-15}\,\mathrm{erg\,(cm^2\,s\,sr)^{-1}}}\right]. \quad (10)$$

2.1 Modelling the dark matter halo of the Galaxy

The DM halo of the Galaxy has been extensively studied (see, for example, Kravtsov et al. 1998; Klypin, Zhao & Somerville 2002; Battaglia et al. 2005). Various DM profiles, used to fit observed velocity distributions, differ the most in the GC region.

Klypin et al. (2002) and Battaglia et al. (2005) have shown that the DM halo of the Milky Way can be described by the Navarro–Frenk–White (NFW) profile (Navarro, Frenk & White 1997)

$$\rho_{\mathrm{NFW}}(r) = \frac{\rho_{\mathrm{s}} r_{\mathrm{s}}^3}{r(r + r_{\mathrm{s}})^2}, \quad (11)$$

with parameters given in Table 1. The relation between virial parameters and ρ_{s} and r_{s} can easily be found (see, for example, appendix A of Boyarsky et al. 2007a).

To explore the uncertainty of the DM density profile in the inner part of the Galaxy, we also describe the DM distribution in the Milky Way using an isothermal profile (Bahcall & Soneira 1980):

$$\rho_{\mathrm{iso}}(r) = \frac{v_{\mathrm{h}}^2}{4\pi G_N} \frac{1}{r^2 + r_{\mathrm{c}}^2} = \frac{\rho_0}{1 + (r/r_{\mathrm{c}})^2}. \quad (12)$$

The following parameters of the isothermal profile reproduce the DM contribution to the (outer parts of) Galaxy rotation curve $v_{\mathrm{h}} = 170\,\mathrm{km\,s^{-1}}$ and $r_{\mathrm{c}} = 4$ kpc (Boyarsky et al. 2006c, 2007a), that is

$$\rho_0 = 1.2 \times 10^6\,\mathrm{keV\,cm^{-3}} \left(\frac{v_{\mathrm{h}}}{170\,\mathrm{km\,s^{-1}}}\right)^2 \left(\frac{4\,\mathrm{kpc}}{r_{\mathrm{c}}}\right)^2.$$

These parameters are consistent with those from favoured NFW models of Klypin et al. (2002) and Battaglia et al. (2005); that is, for $\phi \geqslant 90^\circ$ the difference between the isothermal model and the NFW model with preferred parameters was completely negligible (less than 5 per cent; see Fig. 5). Both types of model give the local DM density at the position of the Sun to be $\rho_{\mathrm{DM}}(\mathrm{r}_\odot) \simeq 0.22\,\mathrm{GeV\,cm^{-3}}$, which is close to existing estimates (Kuijken & Gilmore 1989a,b,c, 1991; Gilmore, Wyse & Kuijken 1989).

The DM flux from a given direction ϕ, measured by an observer on Earth (at a distance $\mathrm{r}_\odot \simeq 8.5$ kpc from the GC), is given by

$$\mathcal{S}_{\mathrm{iso}}(\phi) = \frac{\rho_0 r_{\mathrm{c}}^2}{R} \times \begin{cases} \frac{\pi}{2} + \arctan\left(\frac{\mathrm{r}_\odot \cos\phi}{R}\right), & \cos\phi \geqslant 0 \\ \arctan\left(\frac{R}{\mathrm{r}_\odot |\cos\phi|}\right), & \cos\phi < 0 \end{cases}, \quad (13)$$

where $R = \sqrt{r_{\mathrm{c}}^2 + \mathrm{r}_\odot^2 \sin^2\phi}$ and $\rho_0\, r_{\mathrm{c}} \simeq 1.5 \times 10^{28}\,\mathrm{keV\,cm^{-2}}$.

The uncertainty of the DM radial density profile in the inner Galaxy stems from the difficulty of separation between visible and DM contributions to the inner Galaxy rotation curve.[6] In order to obtain the most conservative limit on the column density of the DM in the direction of the GC, we can assume the following 'rigid lower bound': while the DM outside $\mathrm{r}_\odot$ is described by the 'maximal disk' model (model A_2 of Klypin et al. 2002), for $r \leqslant \mathrm{r}_\odot$ the DM density remains constant (so that the total DM mass within $\mathrm{r}_\odot$ is the same as in the model A_2 of Klypin et al. 2002). This gives

$$\rho_{\mathrm{DM}}^{\mathrm{min}} \simeq 3.9 \times 10^6\,\mathrm{M_\odot\,kpc^{-3}} = 0.146 \times 10^6\,\mathrm{keV\,cm^{-3}}. \quad (14)$$

The surface brightness profile on the 'constant density' model is shown by the black dashed line in Fig. 5. We can see that the difference between the maximal ($\phi = 0^\circ$) and the minimal $\phi = 180^\circ$) column densities is ~3.4 (compared to ~6 for the isothermal model). For comparison, we show in Fig. 5 the expected DM flux (equation 6) for various profiles. The minimal column density is, of course, that in the direction of the anticentre: $\mathcal{S}(\phi = 180^\circ) \simeq 0.33 \times 10^{28}\,\mathrm{keV\,cm^{-2}}$. We see that even for the minimal profile $S(\phi < 30^\circ) \geqslant 10^{28}\,\mathrm{keV\,cm^{-2}}$.

[6] When quoting the results of Klypin et al. (2002), we do not take into account the effects of baryon compression on DM. While these effects make DM distribution in the core of the Milky Way more dense, any such computation is strongly model-dependent.

Table 1. Best-fitting parameters of the NFW model of the Milky Way DM halo. The maximum disk model maximizes the amount of baryonic matter in the inner 3 kpc of the Milky Way halo [$M_{\rm DM}/(M_{\rm disk}+M_{\rm bulge})=0.4$ for model A_2 and $M_{\rm DM}/(M_{\rm disk}+M_{\rm bulge})=0.14$ for model B_2].

References	$M_{\rm vir}(\rm M_\odot)$	$r_{\rm vir}$ (kpc)	Concentration	$r_{\rm s}$ (kpc)	$\rho_{\rm s}$ ($\rm M_\odot$ kpc^{-3})
Klypin et al. (2002), favoured models (A_1 or B_1)	1.0×10^{12}	258	12	21.5	4.9×10^{6}
Klypin et al. (2002), maximum disk models A_2	0.71×10^{12}	230	5	46	0.6×10^{6}
Klypin et al. (2002), maximum disk models B_2	0.71×10^{12}	230	10	23	3.1×10^{6}
Battaglia et al. (2005)	$0.8^{+1.2}_{-0.2}\times10^{12}$	255	18	14.2	11.2×10^{6}

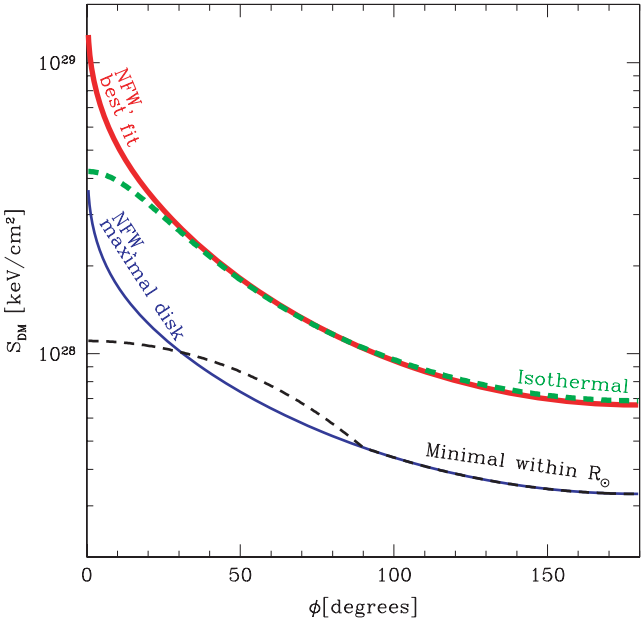

Figure 5. Expected column density for various DM profiles: favoured NFW profile (red thick solid line); NFW profile with the maximal disk (model A_2; see Table 1; blue solid line); cored (isothermal) profile (green thick dashed line); constant density within $\rm r_\odot$ (black dashed line).

2.2 Dark matter decay line count rate

In the case of the Majorana sterile neutrinos of mass $M_{\rm DM}$, the DM decay width is given by (Pal & Wolfenstein 1982; Barger, Phillips & Sarkar 1995):[7]

$$\Gamma_{\rm DM}\simeq 1.3\times10^{-32}\left(\frac{\sin^2 2\theta}{10^{-10}}\right)\left(\frac{M_{\rm DM}}{1\,\rm keV}\right)^5 \rm s^{-1}. \quad (15)$$

Substituting equation (15) into equation (6) we find

$$\frac{{\rm d}F_{\rm DM}}{{\rm d}\Omega}(\phi)\simeq 8.3\times10^{-15}\rm erg\,(cm^2\,s\,sr)^{-1}\times\left(\frac{\sin^2 2\theta}{10^{-10}}\right)\left(\frac{M_{\rm DM}}{1\,\rm keV}\right)^5\left[\frac{\mathcal{S}_{\rm DM}(\phi)}{10^{28}\,\rm keV\,cm^{-2}}\right]. \quad (16)$$

The lower bound on the DM decay line rate in SPI pointings toward the inner Galaxy is calculated by substituting the column density $\mathcal{S}=10^{28}\,\rm keV\,cm^{-2}$ (see Fig. 5) into equations (10) and (16):

$$F_{\rm min}\simeq 3.0\times10^{-6}\rm cts\,cm^{-2}\,s^{-1}\left[\frac{\mathcal{S}_{\rm DM}(\phi)}{10^{28}\rm keV\,cm^{-2}}\right]\times\left(\frac{\sin^2 2\theta}{10^{-10}}\right)\left(\frac{M_{\rm DM}}{1\,\rm keV}\right)^4. \quad (17)$$

The approximation of the constant surface brightness works well, if the extended source has a core of angular diameter exceeding the size of the SPI PCFOV ($\Theta_{\rm PCFOV}\approx17^\circ$ maximal off-axis angle). Taking the isothermal profile, the angular size of the flat core of the extended source is

$$\phi_{\rm core}=\arctan(r_{\rm c}/\rm r_\odot)\simeq 25^\circ, \quad (18)$$

which satisfies this constraint.

3 STRATEGY OF SEARCH FOR THE DARK MATTER DECAY LINE WITH SPI

The Milky Way halo contribution to the DM decay signal represents the all-sky source. Indeed, as the results of Section 2.1 show, the variability of the signal over the sky may be as low as a factor of ∼3. This makes the strategy for searching for the DM decay signal different from any other type of astrophysical source: the point sources, diffuse sources (e.g. ∼10° Gaussian profile for the $\rm e^+$ $\rm e^-$ annihilation region; Knödlseder et al. 2005) or even the search for the DM annihilation signal (see, for example, Boehm et al. 2004; Tasitsiomi, Gaskins & Olinto 2004; Carr, Lamanna & Lavalle 2006; Diemand, Kuhlen & Madau 2007; Sánchez-Conde, Prada & Łokas 2006).

The problem is exacerbated by the fact that during its motion, SPI is irradiated by charged high-energy particles (particles from the Earth's radiation belt, solar wind, cosmic TeV photons). As a result, the materials (even the detectors themselves) used for SPI construction start to radiate in different energy regions (see Section 3.2). As a result, any SPI spectrum consists of a broad continuum, which is a combination of the sky and instrumental backgrounds, and of a set of the instrumental background lines (Attié et al. 2003; Diehl et al. 2003; Jean et al. 2003; Weidenspointner et al. 2003). In order to detect a spectral line produced by an astrophysical source, we have to be able (i) to separate the continuum and line contributions to the spectrum and (ii) to separate the instrumental and sky signal contributions from the lines found.

We can expect three a priori situations, as follows.

(1) The DM decay line is strong (its equivalent width much larger than the spectral resolution) and at its position there are no other strong lines (of either instrumental or astrophysical origin). Such a line, because of its presence in any SPI spectrum and its low variability over the sky, can in principle be confused with some unknown instrumental line.

[7] The quoted value of $\Gamma_{\rm DM}$ is for the Majorana sterile neutrino. For the Dirac particle, this value is two times smaller (cf. Pal & Wolfenstein 1982; Barger et al. 1995).

(2) The DM line is weak ($\sim$3–4σ detection over the continuum) but also its position does not coincide with any instrumental line.

(3) The DM decay line coincides with some instrumental line. To be able find such a line, we need to model the instrumental background of SPI.

To be able to work effectively with all these situations, we need to find a way to separate the source and background contributions.

3.1 Imaging

To distinguish source and background contributions to the signal, the imaging capabilities of an instrument are often used. If the size of a point or even an extended source on the sky is smaller than the size of the SPI FOV, we can (at least, to some extent) use the imaging capabilities of the SPI instrument. In this case, the coded mask, placed above the detector, partially screens the individual detectors from the source. Thus, the source at a given position on the sky produces different count rates in different detectors. We can find the source flux by comparing the ratios of the actual count rates in different modules of the detector to those predicted by the degree of screening of the modules by the mask (see Skinner & Connell 2003; Dubath et al. 2005). It is a challenge, however, to use the imaging capabilities of the SPI to separate the astrophysical signal from the instrumental background, if the size of the extended source is comparable to the size of the SPI FOV (see, for example, Knödlseder et al. 2005; Allain & Roques 2006; Weidenspointner et al. 2007, and references therein). Therefore, for our analysis we did not use any imaging capabilities of SPI, and to produce spectra from some point in the sky we just collected all the photons arriving in the SPI FOV.

3.2 SPI background modelling

In the absence of imaging, the separation of the instrumental and astrophysical contributions to the line spectrum requires some sort of background modelling (see, for example, Weidenspointner et al. 2003; Teegarden et al. 2004; TW06). Namely, for the background modelling we can use the fact that for any DM distribution model the intensity of the DM decay line changes by a factor of $\geqslant$3 between the pointings towards the GC ($\phi \sim 0^\circ$) and anticentre ($\phi \sim 180^\circ$; see Section 2.1). However, if the line is of purely instrumental origin, there is no a priori reason why the strength of the line in the background spectra of the pointings towards, for example, the Galactic anticentre should be different from the strength of the line in the spectra of the pointings towards, for example, the GC. Thus, one possible way to distinguish between the DM decay and the instrumental origin of the line is to study the variations of the line's strength depending on its sky position (in the simplest case, on the 'off-GC' angle ϕ, of the pointing; equation 5).

The situation becomes more complicated because the instrumental background (and thus the intensity of the instrumental lines) experiences great variability in time (depending on the position in orbit, on solar flares and the solar activity period, on the degradation of the detectors, etc.; see Jean et al. 2003; Teegarden et al. 2004). As observations of different parts of the sky can be significantly separated in time, it is necessary to use 'background tracers' to find the correct spatial dependence of the line intensity (Jean et al. 2003; TW06). Without some sort of 'renormalization' procedure, which corrects the absolute value of the line flux using a measurement of the specific characteristics of the SPI instrument as a 'calibrator' of the flux, the ϕ dependence for any of the detected lines contains no useful information. There are various 'background tracers': Ge detector saturation rates, anticoincidence shield rates, rates of certain background lines (see Jean et al. 2003; Teegarden et al. 2004; TW06, and references therein).

3.3 Searching for the lines

To be able to detect a strong DM line, which is not close in position to any instrumental line (case 1 above), we used the modification of the method of background subtraction, described in TW06. TW06 looked for γ-ray lines, assuming different types of sources, from point sources to very diffuse sources (10° Gaussian, 30° flat, etc.). TW06 showed that the strong background line at 198 keV can be used as a background tracer, if background observations are matched close in time to the corresponding 'source' observations. This allowed TW06 to cancel all strong instrumental lines with a precision better than 1 per cent. TW06 detected no emission line in such a background-subtracted spectrum (apart from 511 and 1809 keV) with a significance above 3.5σ.

We adopt the following modification of the TW06 method.

(i) As the DM decay signal remains nearly constant within the central 30–50°, the method of TW06, if applied directly, could cancel most of the DM signal.[8] We therefore subtract the data (renormalized by the strength of the 198-keV line) in a direction away from the GC (off-GC angle $\phi > 120^\circ$) from the ON-GC data set (angle $\phi \leqslant 13^\circ$).

(ii) In the resulting 'ON–OFF' spectrum, we perform a search for the line with a significance higher than 3σ.

This procedure allows us to eliminate strong instrumental lines with a precision better than a few per cent. At the same time, any strong DM line would remain in the 'ON–OFF' spectrum. Indeed, even for the flattest profile (Section 2.1), the strength of the DM signal in the OFF data set is at least 60 per cent weaker than that of the ON data set. Therefore, we see that the modification described above is indeed well suited to a search for the strong DM decay line (case 1).

However, this method does not work well for weak (3–4σ) lines, or for lines whose positions coincide with some instrumental line (cases 2 and 3 above). Indeed, in this case it is not possible to tell whether the remaining line is the residual of the instrumental line or has an astrophysical origin. Below, we use an alternative method of analysis for the detected lines, suitable for cases (2) and (3).

3.4 Analysing a candidate line

Having detected a number of lines with a significance of 3σ and above, we should decide which of these can be considered as 'DM decay line candidates'. To this end, we perform the following.

(i) We compare line flux for each of these lines with the flux of the same line in the 'ON' spectrum. We decide that the line is a 'DM line candidate' if the cancellation of the flux between ON and OFF data sets is worse than 10 per cent.[9]

[8] For example, for the most conservative DM distribution model, the difference of DM signals at $\phi = 0^\circ$ and $\phi = 30^\circ$ is only 8 per cent.

[9] In principle, the DM line in the ON–OFF spectrum should not cancel by more than $\sim$40 per cent, while the background instrumental line should cancel better than 1 per cent. Thus, choosing the threshold to be around 10 per cent ensures that no DM decay line is thrown away while most of the instrumental lines disappear.

(ii) For any 'DM candidate line' we construct its 'spatial profile' (as described in detail in Section 4) to check for the possibility of it being a DM decay line (we also construct the distribution of the line flux over the sky for all unidentified lines from Weidenspointner et al. 2003). Because the column density of the DM in the direction towards the GC should be higher than that in the direction toward the Galactic anticentre, we should see a gradual decrease of the line strength with increasing angle ϕ. We do not make any specific assumption about the DM density profile and do not try to fit the candidate line spatial profile to any particular model. Rather, we see if there is a general trend of decreasing intensity of the line with the increasing off-GC angle.

4 DATA REDUCTION

4.1 ON data set

During its almost five years in orbit *INTEGRAL* has intensively observed the inner part of the Galaxy (the GC, the Galactic bulge and the inner part of the Galactic plane) and has collected about $T_{\rm exp} \sim 10$ Ms of exposure time in the GC region. In our analysis of the inner Galaxy, we have used the publicly available data (as of 2007 July) from all *INTEGRAL* pointings at which the angle off the GC was at most 13° and for which the SPI exposure time was larger than 1 ks. These criteria select 5355 pointings (or 'Science Windows', ScWs), with a total exposure time of 12.2 Ms, spread over the period from 2003 February to 2006 April 25. We call this data set the 'ON' data set.

For each of the analysed ScWs, we have extracted photon (event) lists from SPI-OPER.FITS files and applied an additional energy correction to convert the channel number into photon energy, using the SPI_GAIN_COR tool from standard Offline Analysis Software (OSA). We have binned the events into narrow energy bins of the size $\Delta E_{\rm bin} = 0.5$ keV to generate the background count spectra in each ScW, each revolution and, subsequently, in the entire data set.

We then applied the 'sliding spectral window' method to the line search (as described, for example, in TW06 to produce a continuum-subtracted spectrum of the 'ON' data set. Namely, at each given energy E_0, we define an energy interval $E_0 - 2\Delta E < E < E_0 + 2\Delta E$, where ΔE is the SPI spectral resolution at a given energy, as a 'line signal' energy band. For the (energy-dependent) ΔE, we used an approximate formula from the SPI/*INTEGRAL* ground calibration of the FWHM (Attié et al. 2003):

$$\Delta E(E) = F_1 + F_2\sqrt{E} + F_3 E \tag{19}$$

where $F_1 = 1.54$, $F_2 = 4.6 \times 10^{-3}$, $F_3 = 6.0 \times 10^{-4}$ and energy E is in keV. For $E = 10^3$ keV FWHM ≈ 2.3 keV.

For each energy bin centred at an energy E_0, we have defined the two adjacent energy intervals, $E_0 - 4\Delta E < E < E_0 - 2\Delta E$ and $E_0 + 2\Delta E < E < E_0 + 4\Delta E$. We have postulated that the sum of the count rates in these two adjacent energy bands gives the measure of the continuum count rate in the energy band around E_0. Subtracting the sum of the count rates in the adjacent energy bands from the count rate in the 'line signal' energy band, we have calculated the continuum-subtracted count rate at a given energy E_0. Performing such a procedure at all energies 20 keV $< E_0 <$ 8 MeV, we have produced a 'continuum-subtracted' SPI background spectrum. In this spectrum, we are able to identify most of the known instrumental lines (Weidenspointner et al. 2003).

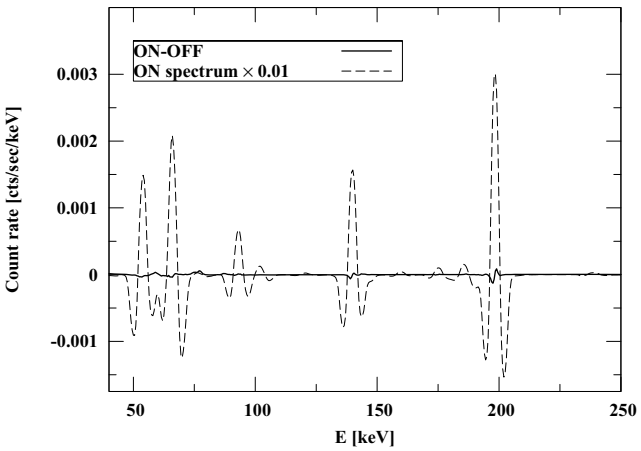

Figure 6. Comparison of the ON–OFF spectrum (thick solid line) with the $0.01\times$ ON spectrum after the sliding window (thin dashed line). It can be seen that the instrumental lines are subtracted with a precision better than 1 per cent.

4.2 ON–OFF data set

Most of the lines found in the continuum-subtracted background spectrum are of instrumental origin. To remove these, we matched each ScW in the ON data set with the pointing away from the GC (galactic coordinate $\phi > 120°$) – OFF pointing. As described by TW06, the 198-keV line can serve as a good background tracer if the time duration between ON and OFF observations is $\leqslant$20 d. We were able to match 3688 ON–OFF pairs. For each ON–OFF pair, we introduced a normalizing coefficient n for the OFF spectrum in such a way that the strong instrumental line at 198 keV cancelled completely after subtraction of the OFF spectrum multiplied by the factor n from the ON spectrum. After this, we subtracted (renormalized) the OFF ScW from the corresponding ScW from the ON data set. This allowed us to remove most prominent instrumental lines with a precision better than 1 per cent (see Fig. 6). To avoid contributions of strong astrophysical sources (such as the Crab nebula) we discarded all pairs with negative total flux in the 20–40 keV range after subtraction. Taking the average over the 2456 remaining 'good' pairs, we obtained a spectrum almost free from background at energies above 200 keV. At low (<200 keV) energies we found a continuum component, which can be fitted with the simple power law:

$$F(E) = F_0 \left(\frac{E}{100\,\text{keV}}\right)^{\alpha}. \tag{20}$$

The parameters of this background were found to be

$$F_0 = (4.95 \pm 0.05) \times 10^{-5}\,\text{cts}\,\text{s}^{-1}\text{cm}^{-2}$$
$$\alpha = -(2.264 \pm 0.003). \tag{21}$$

This continuum represents the residual contribution from the whole set of astrophysical sources present in the Galactic bulge.

4.3 Systematic error

To estimate the systematic error of our 'ON-minus-OFF' data set, we computed the background around the 'tracer line' at 198 keV. We found that it does not vanish. Thus, we estimated the systematic error as the error in the normalization coefficient n, which would make the background zero within systematic uncertainty. This correction δn can be found as follows. Let n be the coefficient, necessary to

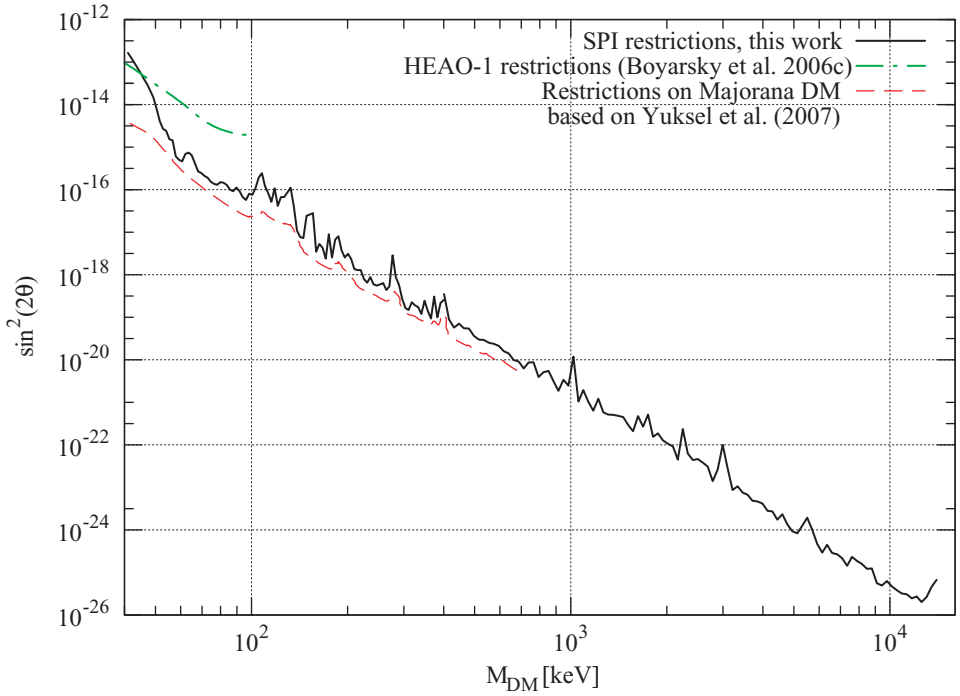

Figure 7. Upper bound on the mixing angle of the DM sterile neutrino as a function of the sterile neutrino mass, obtained from the analysis of the background spectrum of the pointings toward the inner 13° of the Galaxy. For masses $\leqslant$700 keV, the restrictions from Y07 (divided by a factor of 2, because of the Majorana nature of the DM) are also shown by a dashed line (see Section 6). For masses <100 keV, the previous restrictions from HEAO-1 (Boyarsky et al. 2006c) are also shown. The region above the curve is excluded.

cancel flux in the 198-keV line in the ON and OFF spectra:

$$n = F_{\rm ON}/F_{\rm OFF}. \tag{22}$$

Here, $F_{\rm ON}$ and $F_{\rm OFF}$ are fluxes in the 198-keV line in the ON and OFF ScWs, respectively. The remaining non-zero δF flux in the adjacent to line position in the ON–OFF spectrum determines the uncertainty of the coefficient:

$$\delta n = \frac{\delta F}{F_{\rm ON}}. \tag{23}$$

We found that the average value of $\langle \delta n \rangle$ is equal to $\langle \delta n \rangle = 1.1 \times 10^{-3}$, $\langle n \rangle \sim 1$. So, our systematic error of the final ON–OFF spectra at energy E is $1.1 \times 10^{-3}\, F_{\rm OFF}(E) \approx 1.1 \times 10^{-3} F_{\rm ON}$. We add this systematic uncertainty to the flux of the ON–OFF spectrum in every energy bin.

4.4 Obtaining 3σ restrictions

For energies at which no lines were detected (i.e. the 'continuum-subtracted' count rate did not deviate by more than 3σ from zero), we obtained the 3σ upper limit on the possible flux from the DM decay. Above ~200 keV, the flux in the energy bin is zero within statistical errors. Therefore, the 3σ upper limit flux is given by statistical plus systematic errors. Below 200 keV, we put statistical restrictions above the power law continuum flux (21), described in Section 4.2. Using equation (17) we can derive the restriction on the sterile neutrino mixing angle, implied by this upper limit. It should be also noted that the subtraction of the OFF observations led to the reduction of the expected DM signal. Taking the most conservative 'minimal' model, described in Section 2.1, we see that the subtraction of the OFF signal leads to about a 40 per cent decrease of the expected DM signal.[10] The resulting 3σ bound is shown in Fig. 7.

4.5 Possible dark matter candidates

When analysing the ON–OFF spectrum, we found that almost all lines present in the ON spectrum cancel with a precision better than a few per cent. We found 21 lines (see Table 3) that did not cancel by at least 90 per cent (including known lines at 511 and 1809 keV). Apart from these two lines, all other lines are detected with low significance 3–4σ.

As discussed in Sections 3.3 and 3.4, we took all these lines as possible DM candidates and analysed the dependence of the line fluxes $F(\phi)$ on the off-GC angle ϕ of the pointing. If the DM distribution in the inner part of the Galaxy were known, it would be possible to distinguish between the instrumental and DM decay origin of a line by fitting $F(\phi)$ with a known profile calculated from the radial DM density profile. However, the details of the radial DM density profile in the inner Galaxy are highly uncertain, and this prevents us from directly fitting the model profile to the data. We adopted a simple criterion, which selects a DM decay candidate line: the ratio of fluxes

$$\mathcal{R} = \frac{F(0^\circ)}{F(180^\circ)} \geqslant \mathcal{R}_{\rm min} \simeq 3. \tag{24}$$

Here, $\mathcal{R}_{\rm min}$ is the ratio of the DM decay line fluxes from the GC and the Galactic anticentre in the 'minimal DM content' model of DM distribution.

[10] To estimate this, we took the maximal column density for OFF observations at $\phi = 120^\circ - 17^\circ$.

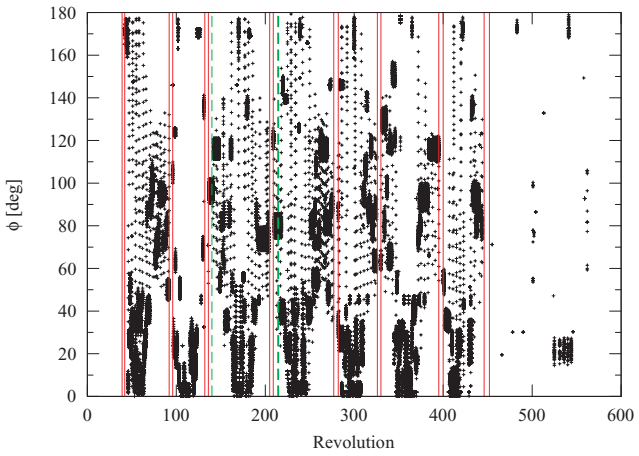

Figure 8. Position on the sky as a function of revolution over six years of *INTEGRAL* observations. The periods of annealing phases are shown by solid vertical lines. Two dashed lines indicate the revolution, during which detectors 2 and 17 of the 19 SPI detectors failed.

Table 2. Splitting revolutions into phases in correspondence with annealing phases and breakage of the detectors (revolutions, marked with*).

Phase	Revolutions (start–stop)
1	042–092
	096–140*
2	140–205
	209–215*
3	215–277
4	282–326
5	330–395
6	400–446

Because the observations at different off-GC angles are carried out during different time periods, to properly study the dependence of the line flux on the off-GC angle ϕ, we should take into account the time variability of the response of the SPI detectors. Several factors have to be taken into account. First, the SPI instrument goes through a so-called 'annealing' phase, a heating of the detectors to recover from radiative damage.[11] Next, two of the 19 SPI detectors have 'died'.[12] The failed detectors also affect the response of their neighbours. To marginalize the effects of the changing response of the SPI detector, we split the entire data set into seven periods, as shown in Fig. 8. The intervals are summarized in Table 2. As both detector failures occurred soon after the end of an annealing phase, we chose to ignore revolutions 136–140 and 209–215. The period 096–140 does not cover the essential part of the sky and therefore we skip this, leaving only six periods.

For each of the periods shown in Table 2, we plot the distribution of the line flux as a function of the off-GC angle ϕ. The results are summarized in Fig. 9. We can see that none of these lines exhibits a clear trend of decreasing from $\phi = 0^\circ$ to $\phi = 180^\circ$. For each line (and each phase), we also compute the average flux $\bar{F}$, the standard deviation σ_F from the average and the minimum ($F_{\min}$) and

[11] For details, see the SPI User Manual at http://isdc.unige.ch/Instrument/spi/doc/spi_um.

[12] Detector 2 at revolution 140 and detector 17 at revolutions 214–215.

Table 3. Lines detected in the ON–OFF spectrum with a significance $\geqslant 3\sigma$. Lines marked with† cancel worse than 90 per cent in the ON–OFF spectrum (compared with their flux in the ON spectrum) and thus represent a 'DM candidate'. The 'Identification' column indicates the probable identification of the line in Weidenspointner et al. (2003). Lines marked with '?' are not identified in Weidenspointner et al. (2003), and lines marked with '??' are not present in Weidenspointner et al. (2003).

E (keV)	Significance, σ	ΔE (keV)	Identification
68.5	11.4	0.65	66.7 Ge complex
76.5	58.8	1.10	75 Bi K_α
87	21.2	0.90	87 Bi K_β
94	5.2	0.55	91–105 GaZn
134.5	15.5	0.90	132–140 Ge complex
143	12.6	1.20	140–147 Ge complex
177	3.9	0.95	175 AsGe
186.5	7.3	1.10	184.6 GaZn
193	24.8	0.75	190–198 Ge complex
200	29.3	0.60	198–215 Ge complex
205.5	5.4	0.50	198–215 Ge complex
240	3.4	1.10	238 PbBi
302	3.9	0.70	301.5 GaZn
311.5	7.4	1.10	309.8 GaZn+K
330.5	3.2	0.55	328=? or 331=PbTl
385.5	3.2	1.45	383=PbTl or??
404.5	5.5	0.95	403 Ga Zn+K
431.5	4.4	0.55	??
440.5	12.4	0.80	438 ZnZn
465	4.3	0.95	470-485 NaNa
511†	52.5	1.25	511 e^+ e^-
576	5.2	0.95	574 GeGa
585.5	7.2	1.10	584.5 GeGa+K
597.5	5.0	1.45	596–610 Ge complex
754	4.7	0.85	751 BiBi
803.5	3.7	0.75	803 BiPb
812	10.6	0.95	810 CoFe
819.5	11.6	0.85	817 CoFe+K
827.5	7.1	0.75	825 PbPb
836	12.1	0.95	834 MnCr
845	6.5	1.30	843 MgAl
874	8.8	1.05	872 GeGa
884	10.0	1.05	882 GeGa+K
913	5.2	1.05	911 AcTh
937†	3.1	0.95	?? or 935=MnCr
990	6.0	0.85	987 PbPb
947†	3.6	1.50	??
1014.5	11.1	1.40	1014 MgAl
1068.5	3.3	1.40	?? or 1063=PbPb
1079	3.3	1.00	1077 = GaZn
1098	6.8	1.05	1095 = ?
1108.5	19.9	1.05	1106 GeGa
1118.5	23.9	1.05	1117 GeGa+K
1127	23.5	0.85	1124.5 ZnCu+K
1234†	4.5	1.40	1231 TaW
1349.5	3.5	0.80	1347 GeGa+K
1368.5	13.2	1.55	1368 NaMg
1719.5†	3.3	1.55	1719 BiPb
1753.5	4.0	1.45	?? or 1758 = ?
1767.5	11.1	1.40	1764 BiPb
1781.5	12.4	1.45	1778 AlSi
1809†	15.2	1.85	1808 Mg
1904	3.2	1.45	1901 = GeGa+K or ??
2212	6.7	2.20	2195-2223 BiPo, Al
2225	5.4	1.10	2223 HD
2322	3.1	1.55	2319 = ?
2583.5	3.5	1.65	2599 = ? or ??

Table 3 – *continued*.

E (keV)	Significance, σ	ΔE (keV)	Identification
2616	5.0	1.90	2614 PbTl
2756	9.5	1.90	2754 NaMg
3002.5	5.1	2.45	2993-3013 Al
3176.5†	3.4	1.95	??
3331†	3.4	2.05	??
3802	3.6	2.10	3800 GaZn+K
4307.5	3.6	3.40	4304 GaZn+K
4454	4.2	8.45	4434 C
4738†	3.5	2.30	??
5186.5†	3.5	2.20	??
5208.5†	4.0	1.95	??
5757†	3.4	2.95	??
6129	20.5	3.25	6128.9 O

maximum ($F_{\max}$). Our analysis shows that (i) 95–100 per cent of all points lie within $3\sigma_F$ from the average (thus, the data are consistent with having a flat spatial profile) and (ii) the scatter of the data ($F_{\max} - F_{\min}$) is much less than its mean value $\langle F \rangle$. Therefore, none of these cannot originate entirely from a DM decay. The corresponding numbers for each line and each phase are summarized in Table 4.

The positron annihilation line at $E = 511$ keV illustrates the situation when a line of astrophysical origin is superimposed on top of the strong instrumental line. In this case, the data can be fitted by the constant, plus some function, depending on the assumed shape of the source. Fig. 10 shows the dependence of the flux of the 511-keV line on the off-GC angle of the SPI pointing. We can see that for pointings with the off-GC angle less than 20° (about the size of the PCFOV of SPI) the 511-keV line flux contains a contribution from a sky source at the position of the GC. However, for the pointing at larger off-GC angles the astrophysical source is not visible and the only contribution comes from the instrumental line, whose flux does not depend on the off-GC angle of the pointing.

5 RESULTS

We analysed the spectrum of SPI and found that none of the strong (i.e. detected with significance above 5σ) lines can be interpreted as those of decaying DM. This conclusion was based on the fact that variability of these lines over the sky is less than 10 per cent (when moving from the GC to the anticentre, see Fig. 11). At the same time, for any realistic DM model such a variability would be greater than at least 60 per cent. Thus, we exclude the possibility that one of the spectral lines detected in the SPI background spectrum is a DM decay line.

The non-detection of a DM decay line in the entire energy range of the SPI detector has enabled us to put an upper limit on the parameters of DM particles. In particular, the 3σ upper bound on the mixing angle of the sterile neutrino DM in the mass range from 40 keV to 7 MeV is shown in Fig. 7.

Our results are applicable to any decaying DM. To this end, we also present the restrictions on the DM lifetime (with respect to the radiative decay) as a function of the energy of emitted photons. The corresponding exclusion plot is shown in Fig. 12. For example, the gravitino can decay into a neutrino and photon (similar to the case of the sterile neutrino) in supersymmetric theories with broken R-parity. Such an interaction is generated by the loop effects (see, for example, Borgani et al. 1996; Lola et al. 2007). The restrictions in Fig. 12 improve the existing bounds on the lifetime of such gravitino DM by several orders of magnitude (see Borgani et al. 1996).

To present our results in a form less dependent on a particular model of DM distribution in the Milky Way, we show the 3σ sensitivity towards the line search in Fig. 13. Note that these results should be used with care, as the sensitivity depends on the assumed spatial profile of the source (because the effective area decreases with the off-axis angle; see the discussion in Section 2). The results presented in Fig. 13 are valid for an extended source with a surface brightness that varies on angular scales larger than (or comparable to) the size of the SPI FOV (black solid line). This plot is analogous to fig. 9 of TW06. However, a direct comparison of fig. 9 of TW06 and Fig. 13 is not possible, as TW06 have assumed a different morphology of the extended source (10° Gaussian). Explicitly taking into account the dependence of the effective area of the SPI detector on the off-axis angle (see Section 2), we can find that in order to make a direct comparison between the two figures, we have to 'rescale' the results of fig. 9 of TW06 by an (energy-dependent) factor of $\approx$1.5. This factor converts the sensitivity for the line, produced by a source with a Gaussian surface brightness profile, into that produced by a source of approximately constant surface brightness (see the red curve in Fig. 13).

We have found a number of weak (with a significance of 3–4σ) lines in the background-subtracted spectrum of SPI. These lines cancel by worse than 90 per cent when subtracting the OFF data set (see Section 4). Apart from this, we have found in the background-subtracted spectrum two lines with high significance – known lines at 511 and 1809 keV. Any of these lines can, in principle, be a DM decay line. We analysed each of these by considering the profile of their intensity over the sky. Our analysis shows that none of these lines could be a pure DM line (as their dependence on the off-GC angle does not show any clear trend of decreasing towards the anticentre). The possibility that some of these lines are the superposition of instrumental and DM lines remains open. Quantitative analysis of the amount of DM flux admissible in a given line depends strongly on the model of DM distribution in the Milky Way halo. Therefore, it was not conducted here.

6 DISCUSSION

The purpose of this work was to understand how to search for a DM decay line with the SPI spectrometer and to check that none of the strong lines present in the SPI background was confused with the DM decay line. Our analysis shows that all the strong lines were, indeed, of instrumental origin. It provides the upper bound on the flux of 'weak' (3–4σ above the background) lines, which leads to corresponding restrictions (see Section 5). To further improve the results, it is necessary to work with the weak lines (or lines coinciding in position with instrumental lines). To do this, we need more sophisticated procedures for subtraction of the instrumental background (e.g. imaging).

One of the most interesting cases of the coinciding instrumental and celestial line is the positronium annihilation line at 511 keV. An excess of positron annihilation emission on top of the strong instrumental line (related to positrons annihilating inside the detector) was noticed long ago (for an incomplete set of references, see for example, Prantzos 1993; Milne et al. 1999; Cheng et al. 1997; Purcell et al. 1997; Knödlseder et al. 2005; Weidenspointner et al. 2006, 2007). There have been many attempts to explain this excess. In particular, it has been attributed to annihilating or decaying DM (see, for example, Boehm et al. 2004; Hooper et al. 2004; Picciotto & Pospelov 2005; Rasera et al. 2006; Boehm, Orloff &

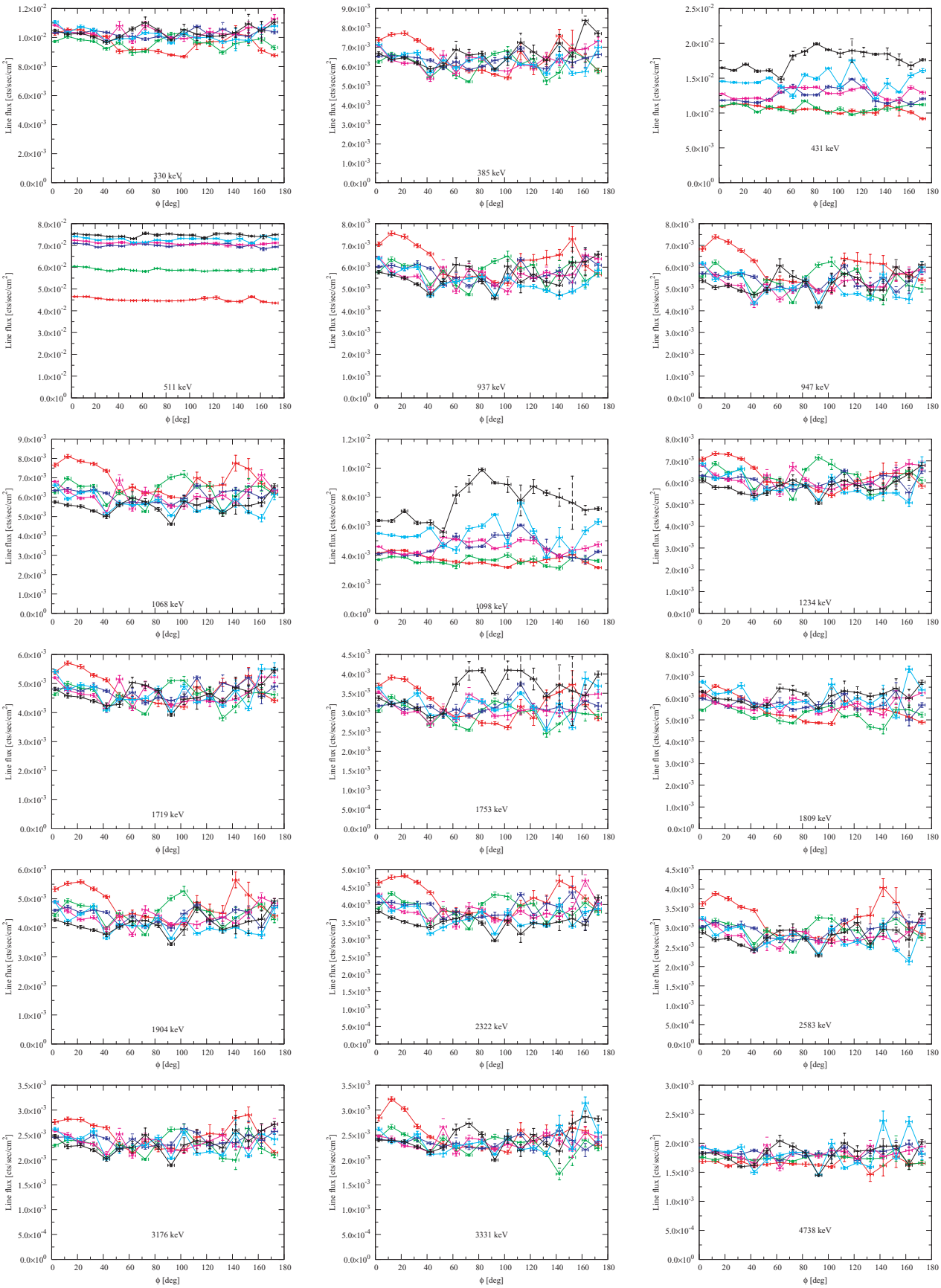

Figure 9. Line flux as a function of the off-GC angle ϕ for the 'candidate' lines from Table 3. For all lines, the flux does not depend on the off-GC angle (with 95–100 per cent of all points lying within three standard deviations from the average). Different colours represent different phases (see Table 2).

Table 4. Characteristics of the spatial profiles of the candidate lines from Table 3. For each line (and for each of the six phases) we compute the average $\langle F \rangle$, the standard deviation (the average scatter of the points around its mean value) σ_F, minimal and maximal values and the ratio of $(F_{\max} - F_{\min})/F_{\min}$, which gives the upper bound on the share of DM present in the given line.

E (keV)	$\langle F \rangle$	σ_F	$F_{\min}$	$F_{\max}$	$\frac{F_{\max}-F_{\min}}{F_{\min}}$
330	9.6e-03	5.8e-04	8.7e-03	1.1e-02	0.23
	9.6e-03	4.0e-04	8.9e-03	1.0e-02	0.15
	1.0e-02	3.4e-04	9.3e-03	1.1e-02	0.16
	1.0e-02	5.2e-04	9.7e-03	1.2e-02	0.23
	1.0e-02	4.7e-04	9.6e-03	1.2e-02	0.24
	1.0e-02	6.1e-04	9.7e-03	1.3e-02	0.33
385	6.6e-03	7.3e-04	5.4e-03	8.0e-03	0.48
	6.1e-03	4.8e-04	5.2e-03	6.8e-03	0.31
	6.3e-03	3.9e-04	5.3e-03	7.1e-03	0.32
	6.2e-03	5.4e-04	5.2e-03	7.4e-03	0.42
	6.2e-03	5.0e-04	5.5e-03	7.6e-03	0.40
	6.7e-03	5.5e-04	5.8e-03	8.4e-03	0.44
431	1.1e-02	5.3e-04	9.2e-03	1.2e-02	0.26
	1.1e-02	5.7e-04	9.5e-03	1.2e-02	0.26
	1.2e-02	1.0e-03	1.0e-02	1.5e-02	0.43
	1.3e-02	8.1e-04	1.1e-02	1.4e-02	0.32
	1.4e-02	1.4e-03	1.2e-02	1.8e-02	0.45
	1.8e-02	1.5e-03	1.4e-02	2.0e-02	0.45
511	4.5e-02	7.8e-04	4.4e-02	4.7e-02	0.07
	5.9e-02	5.8e-04	5.8e-02	6.0e-02	0.04
	7.0e-02	8.5e-04	6.8e-02	7.2e-02	0.05
	7.1e-02	6.7e-04	6.9e-02	7.2e-02	0.04
	7.3e-02	8.7e-04	7.1e-02	7.4e-02	0.05
	7.5e-02	7.4e-04	7.3e-02	7.6e-02	0.03
937	6.3e-03	7.2e-04	5.2e-03	7.7e-03	0.47
	5.8e-03	5.4e-04	4.7e-03	6.6e-03	0.40
	5.7e-03	4.3e-04	4.9e-03	6.5e-03	0.33
	5.6e-03	5.4e-04	4.6e-03	6.6e-03	0.44
	5.3e-03	5.5e-04	4.7e-03	7.5e-03	0.60
	5.5e-03	5.0e-04	4.6e-03	6.6e-03	0.44
947	6.0e-03	7.2e-04	4.9e-03	7.4e-03	0.51
	5.4e-03	5.8e-04	4.4e-03	6.5e-03	0.49
	5.3e-03	4.4e-04	4.4e-03	6.1e-03	0.40
	5.2e-03	5.0e-04	4.3e-03	6.1e-03	0.43
	5.0e-03	6.0e-04	4.3e-03	7.0e-03	0.61
	5.3e-03	5.2e-04	4.2e-03	6.5e-03	0.55
1068	6.9e-03	7.2e-04	5.8e-03	8.2e-03	0.40
	6.3e-03	5.5e-04	5.2e-03	7.3e-03	0.41
	6.1e-03	4.2e-04	5.3e-03	7.0e-03	0.33
	6.0e-03	5.3e-04	5.1e-03	7.2e-03	0.41
	5.6e-03	4.5e-04	4.9e-03	6.8e-03	0.38
	5.5e-03	4.1e-04	4.6e-03	6.6e-03	0.43
1098	3.7e-03	3.9e-04	3.1e-03	4.6e-03	0.49
	3.7e-03	2.5e-04	3.1e-03	4.0e-03	0.30
	4.5e-03	6.6e-04	3.1e-03	6.1e-03	0.95
	4.5e-03	4.8e-04	3.6e-03	5.5e-03	0.56
	5.4e-03	1.0e-03	3.8e-03	7.6e-03	0.99
	7.6e-03	1.3e-03	5.1e-03	9.9e-03	0.94
1234	6.4e-03	5.9e-04	5.4e-03	7.4e-03	0.36
	6.2e-03	5.4e-04	5.2e-03	7.2e-03	0.38
	6.0e-03	3.7e-04	5.2e-03	6.6e-03	0.27
	6.1e-03	4.6e-04	5.4e-03	6.9e-03	0.27
	5.8e-03	5.5e-04	5.1e-03	7.6e-03	0.50
	5.8e-03	4.0e-04	5.0e-03	6.8e-03	0.35
1719	4.9e-03	5.0e-04	4.0e-03	5.7e-03	0.42
	4.6e-03	3.8e-04	3.8e-03	5.1e-03	0.35
	4.7e-03	3.1e-04	3.9e-03	5.2e-03	0.34
	4.6e-03	3.8e-04	4.1e-03	5.4e-03	0.32
	4.5e-03	4.0e-04	3.9e-03	5.5e-03	0.40
	4.7e-03	4.2e-04	3.9e-03	5.7e-03	0.46
1753	3.2e-03	4.1e-04	2.6e-03	4.0e-03	0.53
	3.0e-03	2.7e-04	2.4e-03	3.4e-03	0.41
	3.1e-03	2.7e-04	2.4e-03	3.7e-03	0.59
	3.1e-03	3.0e-04	2.6e-03	3.7e-03	0.43
	3.1e-03	3.5e-04	2.6e-03	3.9e-03	0.51
	3.6e-03	4.5e-04	2.7e-03	4.3e-03	0.61
1809	5.5e-03	5.1e-04	4.6e-03	6.6e-03	0.43
	5.2e-03	3.3e-04	4.6e-03	5.8e-03	0.28
	5.7e-03	3.3e-04	5.0e-03	6.3e-03	0.27
	5.7e-03	3.5e-04	5.2e-03	6.5e-03	0.24
	5.9e-03	4.7e-04	5.0e-03	7.3e-03	0.46
	6.1e-03	3.9e-04	5.4e-03	7.0e-03	0.30
1904	4.8e-03	5.1e-04	4.1e-03	5.6e-03	0.39
	4.5e-03	3.9e-04	3.8e-03	5.3e-03	0.40
	4.4e-03	3.2e-04	3.7e-03	5.2e-03	0.39
	4.3e-03	4.0e-04	3.6e-03	5.2e-03	0.44
	4.1e-03	3.7e-04	3.6e-03	5.2e-03	0.42
	4.1e-03	3.3e-04	3.4e-03	4.9e-03	0.43
2322	4.2e-03	4.0e-04	3.5e-03	4.9e-03	0.39
	3.9e-03	3.0e-04	3.2e-03	4.3e-03	0.34
	3.9e-03	2.9e-04	3.3e-03	4.7e-03	0.42
	3.8e-03	3.2e-04	3.3e-03	4.7e-03	0.43
	3.6e-03	2.9e-04	3.1e-03	4.2e-03	0.35
	3.5e-03	2.8e-04	3.0e-03	4.2e-03	0.42
2583	3.2e-03	4.1e-04	2.6e-03	4.0e-03	0.53
	2.9e-03	2.6e-04	2.4e-03	3.3e-03	0.41
	2.9e-03	2.2e-04	2.4e-03	3.4e-03	0.42
	2.8e-03	2.6e-04	2.4e-03	3.4e-03	0.44
	2.7e-03	2.6e-04	2.1e-03	3.3e-03	0.52
	2.8e-03	2.6e-04	2.3e-03	3.4e-03	0.48
3176	2.5e-03	2.5e-04	2.1e-03	3.0e-03	0.41
	2.3e-03	1.9e-04	1.9e-03	2.7e-03	0.40
	2.4e-03	1.6e-04	1.9e-03	2.7e-03	0.41
	2.4e-03	1.9e-04	2.0e-03	2.7e-03	0.36
	2.3e-03	2.1e-04	1.9e-03	2.7e-03	0.42
	2.3e-03	2.2e-04	1.9e-03	2.9e-03	0.54
3331	2.5e-03	2.9e-04	2.2e-03	3.2e-03	0.50
	2.3e-03	2.0e-04	1.7e-03	2.7e-03	0.55
	2.4e-03	1.5e-04	2.0e-03	2.8e-03	0.35
	2.3e-03	1.7e-04	2.0e-03	2.7e-03	0.33
	2.3e-03	2.1e-04	2.1e-03	3.1e-03	0.51
	2.4e-03	2.3e-04	2.0e-03	2.9e-03	0.44
4738	1.7e-03	6.2e-05	1.5e-03	1.8e-03	0.22
	1.7e-03	6.5e-05	1.5e-03	1.9e-03	0.24
	1.8e-03	9.9e-05	1.5e-03	2.0e-03	0.31

Table 4 – *continued*.

Table 4 – *continued.*

E (keV)	$\langle F \rangle$	σ_F	$F_{\min}$	$F_{\max}$	$\frac{F_{\max}-F_{\min}}{F_{\min}}$
	1.8e-03	1.3e-04	1.5e-03	2.0e-03	0.38
	1.8e-03	2.1e-04	1.5e-03	2.4e-03	0.64
	1.8e-03	1.7e-04	1.4e-03	2.1e-03	0.46
5186	1.5e-03	6.7e-05	1.4e-03	1.7e-03	0.26
	1.6e-03	5.5e-05	1.5e-03	1.8e-03	0.16
	1.8e-03	9.4e-05	1.6e-03	2.1e-03	0.35
	1.8e-03	6.4e-05	1.6e-03	2.0e-03	0.24
	1.8e-03	6.9e-05	1.6e-03	1.9e-03	0.18
	1.8e-03	1.2e-04	1.5e-03	2.0e-03	0.32
5208	1.5e-03	8.8e-05	1.2e-03	1.8e-03	0.51
	1.6e-03	5.6e-05	1.5e-03	1.8e-03	0.21
	1.7e-03	5.8e-05	1.6e-03	1.9e-03	0.16
	1.7e-03	5.3e-05	1.6e-03	1.9e-03	0.15
	1.8e-03	8.0e-05	1.6e-03	2.1e-03	0.28
	1.8e-03	1.3e-04	1.5e-03	2.1e-03	0.39

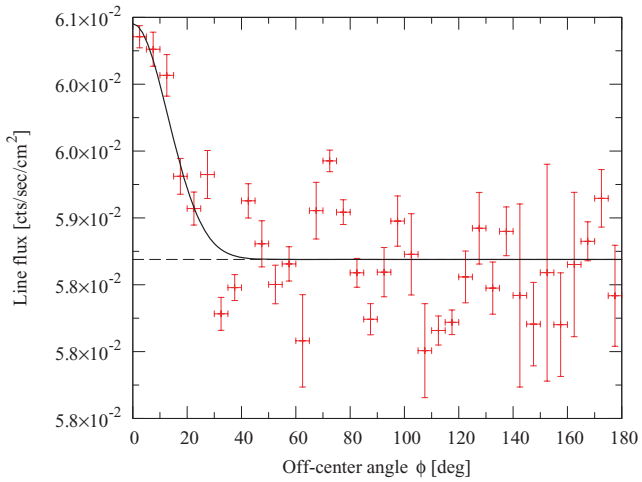

Figure 10. Dependence of the intensity of the positron annihilation line at $E = 511$ keV on the off-GC angle. The solid line shows a fit to the data in the form const $+ N\mathrm{e}^{-\phi^2/(2\sigma^2)}$.

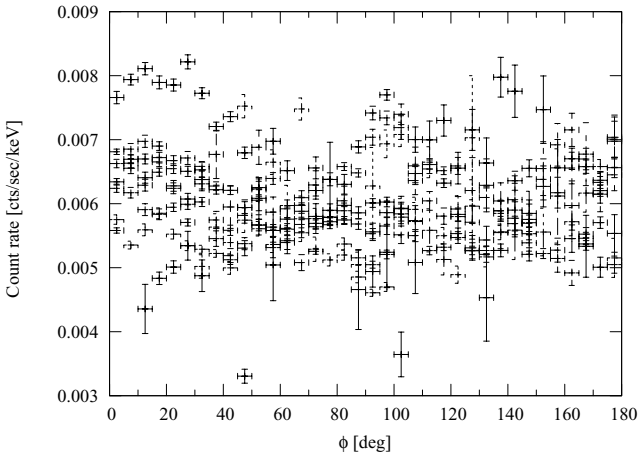

Figure 11. Scatter of the flux data points for the line at $E = 1068$ keV as a function of the off-GC angle.

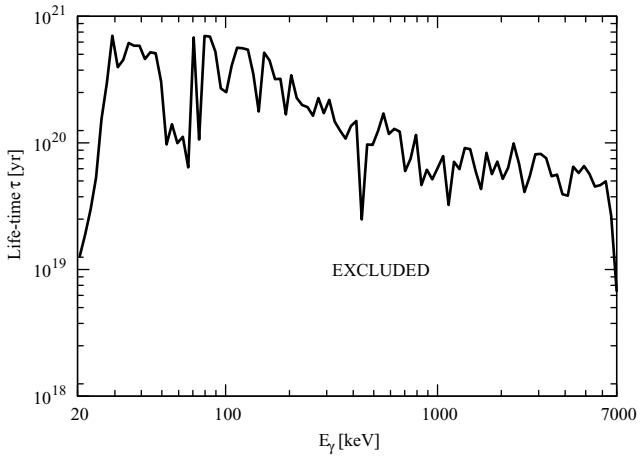

Figure 12. Lifetime of radiatively decaying DM as a function of the emitted photon energy. The region below the curve is excluded.

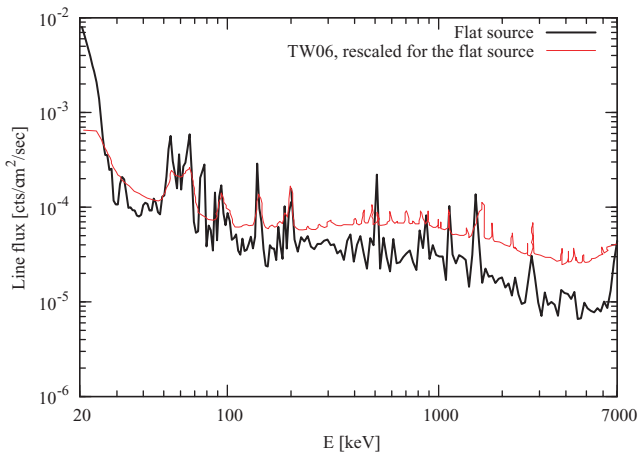

Figure 13. The 3σ sensitivity towards the line search for a flat diffuse source (thick black line). The results of Teegarden & Watanabe (2006, fig. 9) – rescaled to account for the sensitivity towards the flat diffuse source, rather than 10° Gaussian – are shown by the thin red line.

Salati 2006; Frère et al. 2007). The sterile neutrino DM with mass $m_s > 1$ MeV possesses the decay channel $N_s \to e^+e^-\nu$, with positrons annihilating either in flight or at rest, by forming the positronium atom (see, for example, Beacom & Yüksel 2006; Sizun, Cassé & Schanne 2006). Thus, it is possible that the decay of sterile neutrino DM contributes to such a line. A detailed analysis of this case will be given separately.

It should be also mentioned that the region of masses between $20 \lesssim m_{\rm DM} \lesssim 40$ keV remains inaccessible for existing X-ray missions. The strongest restrictions in this region were produced using data from the HEAO-1 mission (Boyarsky et al. 2006c).

When the work on this paper was at its final stage, the work of Y07 was published. Y07 obtained restrictions on the parameters of the sterile neutrino in the range 40–700 keV. To facilitate the comparison, we plot the restrictions of Y07 in Fig. 7 (divided by a factor of 2 to translate them into the restrictions for the Majorana rather than Dirac sterile neutrino DM; see footnote 7). As the data used in our work have about five times longer exposure than the *INTEGRAL* first-year data, on which the results of Y07 are based,

we could have expected results stronger by a factor of ≈2 in our case. However, Fig. 7 shows the opposite. The reason for this is as follows. For the SPI, the sensitivity towards the line search from a particular source depends on the shape of the source. In particular, the results of TW06, on which the work of Y07 was based, were obtained under the assumption of a particular diffuse source (10° Gaussian). As any realistic DM profile is much flatter than the 10° Gaussian, the results of TW06 cannot be applied directly to the case of the DM line search. They should be rescaled to account for the diffuse nature of the DM source (see Section 5). Apart from this, the estimated DM signal from the inner part of the Galaxy is about two times stronger in the work of Y07 than in our work. As the DM signal in the direction of the GC is the most uncertain, we have adopted the conservative flat profile everywhere inside the solar radius, to minimize this uncertainty.

ACKNOWLEDGMENTS

We would like to thank B. Teegarden and K. Watanabe for useful discussions. DM is grateful to the Scientific and Educational Center[13] of the Bogolyubov Institute for Theoretical Physics in Kiev, Ukraine, and especially to V. Shadura, for creating a wonderful atmosphere for young Ukrainian scientists, and to the Ukrainian Virtual Roentgen and Gamma-Ray Observatory VIRGO.UA[14] and computing cluster of Bogolyubov Institute for Theoretical Physics[15] for the use of their computing resources. The work of DM was supported by the Swiss National Science Foundation and the Swiss Agency for Development and Cooperation in the framework of the programme SCOPES – Scientific Cooperation between Eastern Europe and Switzerland. The work of AB was (partially) supported by the European Union Sixth Framework Marie Curie Research and Training Network 'UniverseNet' (MRTN-CT-2006-035863). OR would like to acknowledge the support of the Swiss Science Foundation. This work is also published as CERN-PH-TH/2007-202.

REFERENCES

Abazajian K. N., Markevitch M., Koushiappas S. M., Hickox R. C., 2007, Phys. Rev. D, 75, 063511
Alard C., 1999, A&A, 343, 10
Alcock C. et al., 2000, ApJ, 541, 270
Allain M., Roques J.-P., 2006, A&A, 447, 1175
Asaka, T., Shaposhnikov, M., 2005, Phys. Lett. B, 620, 17
Asaka, T., Laine, M., Shaposhnikov, M., 2007, JHEP, 01, 091
Attié D. et al., 2003, A&A, 411, L71
Avila-Reese V., Colín P., Valenzuela O., D'Onghia E., Firmani C., 2001, ApJ, 559, 516
Bahcall J. N., Soneira R. M., 1980, ApJS, 44, 73
Baltz E. A., Murayama H., 2003, JHEP, 5, 67
Barger, V. D., Phillips, R. J. N., Sarkar, S., 1995, Phys. Lett. B, 352, 365
Battaglia G. et al., 2005, MNRAS, 364, 433
Beacom J. F., Yüksel H., 2006, Phys. Rev. Lett., 97, 071102
Berezhiani Z. G., Khlopov M. Y., 1990, Sov. J. Nucl. Phys., 52, 60
Berezhiani, Z. G., Vysotsky, M. I., Khlopov, M. Y., 1987, Sov. J. Nucl. Phys., 45, 1065
Berezhiani Z. G., Vysotsky M. I., Yurov V. P., Doroshkevich A. G., Khlopov M. Y., 1990, Sov. J. Nucl. Phys., 51, 1020
Bergstrom L., 2000, Rep. Prog. Phys., 63, 793
Bertone G., Hooper D., Silk J., 2005, Phys. Rep., 405, 279
Bertone G., Buchmuller W., Covi L., Ibarra A., 2007, JCAP, 11, 003

[13] See http://sec.bitp.kiev.ua.
[14] See http://virgo.bitp.kiev.ua.
[15] See http://grid.bitp.kiev.ua.

Bode P., Ostriker J. P., Turok N., 2001, ApJ, 556, 93
Boehm C., Hooper D., Silk J., Casse M., Paul J., 2004, Phys. Rev. Lett., 92, 101301
Boehm C., Orloff J., Salati P., 2006, Phys. Lett. B, 641, 247
Bond J. R., Efstathiou G., Silk J., 1980, Phys. Rev. Lett., 45, 1980
Bond J. R., Szalay A. S., Turner M. S., 1982, Phys. Rev. Lett., 48, 1636
Borgani S., Masiero A., Yamaguchi M., 1996, Phys. Lett. B, 386, 189
Boyarsky A., Neronov A., Ruchayskiy O., Shaposhnikov M., 2006a, MNRAS, 370, 213
Boyarsky A., Neronov A., Ruchayskiy O., Shaposhnikov M., 2006b, Phys. Rev. D, 74, 103506
Boyarsky A., Neronov A., Ruchayskiy O., Shaposhnikov M., Tkachev I., 2006c, Phys. Rev. Lett., 97, 261302
Boyarsky A., Ruchayskiy O., Markevitch M., 2006d, ApJ, 673, 752
Boyarsky A., Nevalainen J., Ruchayskiy O., 2007a, A&A, 471, 51
Boyarsky A., den Herder J. W., Neronov A., Ruchayskiy O., 2007b, Astropart. Phys., 28, 303
Boyarsky A., Iakubovskyi D., Ruchayskiy O., Savchenko V., 2007c, preprint (arXiv:0709.2301)
Carr J., Lamanna G., Lavalle J., 2006, Rep. Prog. Phys., 69, 2475
Cembranos J. A. R., Feng J. L., Rajaraman A., Smith B. T., Takayama F., 2006, preprint (hep-ph/0603067)
Cerdeno D. G., Choi K.-Y., Jedamzik K., Roszkowski L., Ruiz de Austri, R., 2006, JCAP, 0606, 005
Cheng L. X. et al., 1997, ApJ, 481, L43
Chung D. J. H., Kolb E. W., Riotto A., 1999, Phys. Rev. D, 59, 023501
Crotty P., Lesgourgues J., Pastor S., 2004, Phys. Rev. D, 69, 123007
Dalcanton J. J., Hogan C. J., 2001, ApJ, 561, 35
Dar A., 1995, ApJ, 449, 550
de Rujula A., Glashow S. L., 1980, Phys. Rev. Lett., 45, 942
Diehl R. et al., 2003, A&A, 411, L117
Diemand J., Kuhlen M., Madau P., 2007, ApJ, 657, 262
Dodelson S., Widrow L. M., 1994, Phys. Rev. Lett., 72, 17
Doroshkevich A. G., Khlopov M. I., Klypin A. A., 1989, MNRAS, 239, 923
Dubath P. et al., 2005, MNRAS, 357, 420
Dubovsky S. L., Tinyakov P. G., Tkachev I. I., 2005, Phys. Rev. Lett., 94, 181102
Fogli G. L., Lisi E., Marrone A., Palazzo A., Rotunno A. M., 2006, Prog. Part. Nucl. Phys., 57, 71
Frère J.-M., Ling F.-S., Honorez L. L., Nezri E., Swillens Q., Vertongen G., 2007, Phys. Rev. D, 75, 085017
Gilmore G., 2007, preprint (astro-ph/0703370)
Gilmore G., Wyse R. F. G., Kuijken K., 1989, ARA&A, 27, 555
Gilmore G., Wilkinson M., Kleyna J., Koch A., Wyn Evans N., Wyse R. F. G., Grebel E. K., 2007a, Nucl. Phys. B, 173, 15
Gilmore G., Wilkinson M. I., Wyse R. F. G., Kleyna J. T., Koch A., Evans N. W., Grebel E. K., 2007b, ApJ, 663, 948
Giunti C., 2007, Nucl. Phys. Proc. Suppl., 169, 309
Goerdt T., Moore B., Read J. I., Stadel J., Zemp M., 2006, MNRAS, 368, 1073
Gruber D. E., Matteson J. L., Peterson L. E., Jung G. V., 1999, ApJ, 520, 124
Hannestad S., Raffelt G., 2004, JCAP, 0404, 008
Hansen S. H., Lesgourgues J., Pastor S., Silk J., 2002, MNRAS, 333, 544
Hooper D., Ferrer F., Boehm C., Silk J., Paul J., Evans N. W., Casse M., 2004, Phys. Rev. Lett., 93, 161302
Hui L., Gnedin N. Y., Zhang Y., 1997, ApJ, 486, 599
Jean P. et al., 2003, A&A, 411, L107
Khlopov M. Y., 1997, Cosmoparticle Physics. World Scientific Press, Singapore
Klimentowski J., Lokas E. L., Kazantzidis S., Prada F., Mayer L., Mamon G. A., 2007, MNRAS, 378, 353
Klypin A., Kravtsov A. V., Valenzuela O., Prada F., 1999, ApJ, 522, 82
Klypin A., Zhao H., Somerville R. S., 2002, ApJ, 573, 597
Knödlseder J. et al., 2005, A&A, 441, 513
Koposov S. et al., 2007, ApJ, in press (arXiv:0706.2687)
Kravtsov A. V., Klypin A. A., Bullock J. S., Primack J. R., 1998, ApJ, 502, 48

Kuijken K., Gilmore G., 1989a, MNRAS, 239, 571
Kuijken K., Gilmore G., 1989b, MNRAS, 239, 605
Kuijken K., Gilmore G., 1989c, MNRAS, 239, 651
Kuijken K., Gilmore G., 1991, ApJ, 367, L9
Kusenko A., 2006, Phys. Rev. Lett., 97, 241301
Kuzmin V. A., Tkachev I. I., 1998, JETP Lett., 68, 271
Kuzmin V. A., Tkachev I. I., 1999, Phys. Rep., 320, 199
Lasserre T. et al., 2000, A&A, 355, L39
Lola S., Osland P., Raklev A. R., 2007, Phys. Lett. B, 656, 83
McCammon D. et al., 2002, ApJ, 576, 188
Milne A. P. et al., 1999, Astrophys. Lett. Commun., 38, 441
Moore B., 1994, Nat, 370, 629
Moore B., Quinn T., Governato F., Stadel J., Lake G., 1999, MNRAS, 310, 1147
Navarro J. F., Frenk C. S., White S. D. M., 1997, ApJ, 490, 493
Pagels H., Primack J. R., 1982, Phys. Rev. Lett., 48, 223
Pal P. B., Wolfenstein L., 1982, Phys. Rev. D, 25, 766
Palazzo A., Cumberbatch D., Slosar A., Silk J., 2007, Phys. Rev. D, 76, 103511
Penarrubia J., McConnachie A., Navarro J. F., 2007, ApJ, 672, 904
Petraki K., Kusenko A., 2008, Phys. Rev. D, 77, 065014
Picciotto C., Pospelov M., 2005, Phys. Lett. B, 605, 15
Prantzos N., 1993, A&AS, 97, 119
Purcell W. R. et al., 1997, ApJ, 491, 725
Rasera Y., Teyssier R., Sizun P., Cassé M., Fayet P., Cordier B., Paul J., 2006, Phys. Rev. D, 73, 103518
Riemer-Sørensen S., Hansen S. H., Pedersen K., 2006, ApJ, 644, L33
Roszkowski L., Ruiz de Austri R., Choi K.-Y., 2005, JHEP, 08, 080
Ruchayskiy O., 2007, in Kleinert H., Jantzen R., Ruffini R., eds, Proc. 11th Marcel Grossmann Meeting on General Relativity. World Scientific Press, Singapore
Sánchez-Conde M. A., Prada F., Łokas E. L., 2006, in Munoz C., Yepes G., eds, AIP Conf. Proc. 878, 2nd International Conference on The Dark Side of the Universe. Am. Inst. Phys., New York, p. 125
Seljak U., Makarov A., McDonald P., Trac H., 2006, Phys. Rev. Lett., 97, 191303
Shaposhnikov M., 2007, in Kleinert H., Jantzen R., Ruffini R., eds, Proc. 11th Marcel Grossmann Meeting on General Relativity. World Scientific Press, Singapore
Shaposhnikov M., Tkachev I., 2006, Phys. Lett. B, 639, 414
Shi X.-d., Fuller G. M., 1999, Phys. Rev. Lett., 82, 2832
Simon J. D., Geha M., 2007, ApJ, 670, 313
Sizun P., Cassé M., Schanne S., 2006, Phys. Rev. D, 74, 06314
Skinner G., Connell P., 2003, A&A, 411, L123
Spergel D. N. et al., 2007, ApJS, 170, 377
Strigari L. E., Bullock J. S., Kaplinghat M., Diemand J., Kuhlen M., Madau P., 2007, ApJ, 669, 676
Strumia A., Vissani F., 2006, preprint (hep-ph/0606054)
Tasitsiomi A., Gaskins J., Olinto A. V., 2004, Astropart. Phys., 21, 637
Teegarden B. J., Watanabe K., 2006, ApJ, 646, 965 (TW06)
Teegarden B. J. et al., 2004, in Schönfelder V., Lichti G., Winkler C., eds, ESA SP-552, 5th *INTEGRAL* Workshop on the *INTEGRAL* Universe. ESA Publications Division, Noordwijk, p. 819
Tremaine S., Gunn J. E., 1979, Phys. Rev. Lett., 42, 407
Vedrenne G. et al., 2003, A&A, 411, L63
Viel M., Lesgourgues J., Haehnelt M. G., Matarrese S., Riotto A., 2005, Phys. Rev. D, 71, 063534
Viel M., Lesgourgues J., Haehnelt M. G., Matarrese S., Riotto A., 2006, Phys. Rev. Lett., 97, 071301
Viel M., Becker G. D., Bolton J. S., Haehnelt M. G., Rauch M., Sargent W. L. W., 2008, Phys. Rev. Lett., 100, 041304
Watson C. R., Beacom J. F., Yuksel H., Walker T. P., 2006, Phys. Rev. D, 74, 033009
Weidenspointner G. et al. 2003, A&A, 411, L113
Weidenspointner G. et al., 2006, A&A, 450, 1013
Weidenspointner G. et al., 2007, preprint (astro-ph/0702621)
Yuksel H., Beacom J. F., Watson C. R., 2007, preprint (arXiv:0706.4084)
Zhang L., Chen X., Kamionkowski M., Si Z., Zheng Z., 2007, Phys. Rev. D, 76, 0613013

This paper has been typeset from a TEX/LATEX file prepared by the author.